

# Contributions of natural and anthropogenic sources to ambient ammonia in the Athabasca Oil Sands and north-western Canada

Cynthia Whaley<sup>1</sup>, Paul A. Makar<sup>1</sup>, Mark W. Shephard<sup>1</sup>, Leiming Zhang<sup>1</sup>, Junhua Zhang<sup>1</sup>, Qiong Zheng<sup>1</sup>, Ayodeji Akingunola<sup>1</sup>, Gregory R. Wentworth<sup>2,3</sup>, Jennifer G. Murphy<sup>2</sup>, Shailesh K. Kharol<sup>1</sup>, and Karen E. Cady-Pereira<sup>4</sup>

<sup>1</sup>Air Quality Research Division, Environment and Climate Change Canada, 4905 Dufferin Street, Toronto, Ontario, Canada

<sup>2</sup>Dept of Chemistry, University of Toronto, 80 St George Street, Toronto, Ontario, Canada

<sup>3</sup>Environmental Monitoring and Science Division, Alberta Environment and Parks, 9888 Jasper Ave NW, Edmonton, Alberta, Canada

<sup>4</sup>Atmospheric and Environmental Research (AER), Lexington, Massachusetts, USA

*Correspondence to:* Cynthia Whaley (cynthia.whaley@canada.ca)

**Abstract.** Atmospheric ammonia (NH<sub>3</sub>) is a short-lived pollutant that plays an important role in aerosol chemistry and nitrogen deposition. Dominant NH<sub>3</sub> emissions are from agriculture and forest fires, both of which are increasing globally. Even remote regions with relatively low ambient NH<sub>3</sub> concentrations, such as northern Alberta and Saskatchewan in northern Canada may be of interest because of industrial Oil Sands emissions, and a sensitive ecological system. A previous attempt to model NH<sub>3</sub> in the region showed a substantial negative bias compared to satellite profiles and aircraft observations. Known missing sources of NH<sub>3</sub> in the model were re-emission of NH<sub>3</sub> from plants and soils (bidirectional flux), and forest fire emissions, but the relative impact of these sources on NH<sub>3</sub> concentrations was unknown. Here we have used a research version of the high-resolution air quality forecasting model, GEM-MACH, to quantify the relative impacts of semi-natural (bidirectional flux of NH<sub>3</sub> and forest fire emissions) and direct anthropogenic (Oil Sands operations, combustion of fossil fuels, and agriculture) sources on ammonia concentrations, both at the surface and aloft, with a focus on the Athabasca Oil Sands region during a measurement-intensive campaign in the summer of 2013. The addition of fires and bidirectional flux to GEM-MACH has improved the model bias, slope and correlation coefficients relative to ground, aircraft, and satellite NH<sub>3</sub> measurements significantly.

By running the GEM-MACH-Bidi model in three configurations and calculating their differences, we find that averaged over Alberta and Saskatchewan during this time period an average of 23.1% of surface NH<sub>3</sub> came from direct anthropogenic sources, 56.6% (or 1.24 ppbv) from bidirectional flux (re-emission from plants and soils), and 20.3% (or 0.42 ppbv) from forest fires. In the NH<sub>3</sub> total column, an average of 19.5% came from direct anthropogenic sources, 50.0% from bidirectional flux, and 30.5% from forest fires. The addition of bidirectional flux and fire emissions caused the overall average net deposition of NH<sub>x</sub> across the domain to be increased by 24.5%. Note that forest

fires are very episodic and their contributions will vary significantly for different time periods and regions.

25 This study is the first use of the bidirectional flux scheme in GEM-MACH, which could be generalized for other volatile or semi-volatiles species. It is also the first time CrIS satellite observations of  $\text{NH}_3$  have been used for model evaluation, and the first use of fire emissions in GEM-MACH at 2.5-km resolution.

## 1 Introduction

30 Ammonia ( $\text{NH}_3$ ) is a short-lived pollutant that is receiving global attention because of its increasing concentrations. Emissions of  $\text{NH}_3$  – which are in large part from agricultural fertilizer, livestock (Behera et al., 2013; Environment and Climate Change Canada, 2016), and biomass burning (Olivier et al., 1998; Krupa, 2003) – have not been regulated to the same extent as other nitrogen species.  $\text{NH}_3$  is the only aerosol precursor whose global emissions are projected to rise throughout  
35 the next century (Moss et al., 2010; Lamarque et al., 2010; Ciais et al., 2013).

$\text{NH}_3$  has an atmospheric lifetime of hours to a day (Seinfeld and Pandis, 1998; Aneja et al., 2001). It is a base that reacts in the atmosphere with sulphuric acid ( $\text{H}_2\text{SO}_4$ ) and nitric acid ( $\text{HNO}_3$ ) to form crystalline sulphate, nitrate salts (e.g.,  $(\text{NH}_4)_2\text{SO}_4$ ,  $\text{NH}_4\text{HSO}_4$ ,  $\text{NH}_4\text{NO}_3$ ) and aqueous ions ( $\text{SO}_4^{2-}$ ,  $\text{HSO}_4^-$ ,  $\text{NO}_3^-$ ), (Nenes et al., 1998; Makar et al., 2003) which are significant components of  
40 fine particulate matter ( $\text{PM}_{2.5}$ ) (e.g., Jimenez et al., 2009, Environment Canada, 2001), thus causing health (Pope III et al., 2002; Lee et al., 2015) and climate impacts (IPCC, 2013). A large portion of  $\text{NH}_3$  is readily deposited in the first 4-5 km from its source, but when in fine particulate form (as  $\text{NH}_4^+$ ), its lifetime is days to several weeks (Galperin and Sofiev, 1998; Park et al., 2004; Behera et al., 2013; Paulot et al., 2014) and can be transported hundreds of kilometers (Krupa, 2003;  
45 Galloway et al., 2008; Makar et al., 2009). Deposition of  $\text{NH}_3$  and these aerosols can lead to nitrogen eutrophication and soil acidification (Fangmeier et al., 1994; Sutton et al., 1998; Dragosits et al., 2002; Carfrae et al., 2004).  $\text{NH}_3$  is listed as a Criteria Air Contaminant (Environment and Climate Change Canada, 2017) in order to help address air quality issues such as smog and acid rain.

Modelling can be used to better understand  $\text{NH}_3$  processes. Recent  $\text{NH}_3$  models have focused  
50 on improving bidirectional flux processes and impacts of livestock. Measurements of  $\text{NH}_3$  bidirectional flux include those in Farquhar et al. (1980); Sutton et al. (1993, 1995); Asman et al. (1998); Nemitz et al. (2001), with indirect support for bidirectional flux also in Ellis et al. (2011). Thus, these studies were the motivation for the recent design of parameterizations to describe this important process (Wu et al., 2009; Wichink Kruit et al., 2010; Massad et al., 2010; Zhang et al., 2010;  
55 Zhu et al., 2015; Fu et al., 2015; Hansen et al., 2017). Additionally, satellite observations are providing valuable insight on ammonia concentrations and emissions both on regional and global scales

(Beer et al., 2008; Clarisse et al., 2009; Shephard et al., 2011; Shephard and Cady-Pereira, 2015; Van Damme et al., 2014; Zhu et al., 2013).

The Athabasca Oil Sands region (AOSR), located in the north-eastern part of the province of Alberta, Canada, is a large source of pollution to air (Gordon et al., 2015; Liggio et al., 2016; Li et al., 2017) and ecosystems (Kelly et al., 2009; Kirk et al., 2014; Hsu and Clair, 2015), as well as a source of greenhouse gases (Charpentier et al., 2009) due to mining and processing by the oil industry. While  $\text{NH}_3$  concentrations surrounding the AOSR in northern Alberta and Saskatchewan remain relatively low – around 0.6-1.2 ppbv background (this study and Shephard et al., 2015) – due to low population and lack of agriculture, the northern Alberta and Saskatchewan ecosystems are sensitive to nitrogen deposition (Clair and Percy, 2015; Wieder et al., 2016a, b; Vitt, 2016; Makar et al., 2017), and the modelled background  $\text{NH}_3$  must be correct in order to understand the relative impacts of the oil sands operations. It is important to understand if the AOSR facilities are causing critical levels of  $\text{NH}_3$ , and if not, if any other kinds of sources (e.g., fires, re-emissions) are. A monitoring study from 2005 to 2008 found  $\text{NH}_3$  concentrations near Fort McMurray and Fort McKay (population centers in the vicinity of the oil sands facilities) to be highly variable in space and time with a range of 1.1 to 8.8 ppbv (where the upper end corresponds to  $\text{NH}_3$  levels found in agricultural regions of Canada and the U.S.), with  $\text{NH}_3$  concentrations 1.5-3 $\times$  higher than  $\text{HNO}_3$  concentrations (Bytnerowicz et al., 2010). Hsu and Clair (2016) also found  $\text{NH}_3$  concentrations in the AOSR to be much higher than  $\text{HNO}_3$ ,  $\text{NO}_3^-$ , and  $\text{NH}_4^+$  concentrations (by 5, 23, and 1.8 $\times$ , respectively). Thus,  $\text{NH}_3$  may contribute the largest fraction of deposited nitrogen in the AOSR compared to other nitrogen species. Estimates of deposition of nitrogen compounds in the AOSR are described in Makar et al. (2017) in this issue, however they did not include  $\text{NH}_3$  bidirectional flux or forest fires in their model simulations.

In a previous study by Shephard et al. (2015) it was found that the GEM-MACH air quality forecasting model (Moran et al., 2010, 2013; Makar et al., 2015a, b; Gong et al., 2015), using a domain covering the Canadian provinces of Alberta and Saskatchewan, at 2.5-km resolution, under-predicted summertime tropospheric ammonia concentrations by 0.4-0.6 ppbv (which is 36-100 % depending on altitude - see Fig. 16 in Shephard et al., 2015) in the AOSR when compared to Tropospheric Emission Spectrometer (TES) satellite measurements and aircraft measurements. Having too much modelled  $\text{NH}_x$  deposition is a cause that was ruled out when Makar et al. (2017) showed that GEM-MACH actually underestimates  $\text{NH}_x$  deposition. Underestimating anthropogenic and agricultural emissions was also ruled out as a cause because the GEM-MACH model performs well in southern Canada and the U.S when compared to the U.S. Ambient Ammonia Monitoring Network (AMoN).  $\text{NH}_3$  sources known to be missing from the GEM-MACH model were forest fire emissions and re-emission of deposited  $\text{NH}_3$  from soils and plants (the latter referred to as bidirectional flux, hereafter), which would have the greatest impact in background areas, such as northern Alberta and Saskatchewan. Therefore, these two sources were added to an updated version of GEM-MACH and

model simulations were repeated for a 2013 summer period (12 August to 7 September 2013) during which an intensive measurement campaign occurred. We utilize ground, aircraft and satellite measurements of  $\text{NH}_3$  and related species to evaluate the model and to quantify the impacts of the different sources on atmospheric  $\text{NH}_3$  and its deposition.

Section 2 provides the model description. Section 3 provides a brief description of ammonia measurements during the campaign. Section 4 presents the evaluation of three model scenarios against three different types of measurements (surface, aircraft, and satellite), and Section 5 presents our quantitative assessment on the impacts of different sources of  $\text{NH}_3$  to ambient concentrations and  $\text{NH}_x$  deposition in the region. Our conclusions appear in Section 6.

## 2 GEM-MACH model description

GEM-MACH (Global Environment Multiscale-Modelling Air quality and CHemistry) is an on-line chemical transport model, which is embedded in GEM, Environment and Climate Change Canada (ECCC)'s numerical weather prediction model (Moran et al., 2010). This means that the chemical processes of the model (gas-phase chemistry, plume rise emissions distribution, vertical diffusion and surface fluxes of tracers, and a particle chemistry package including particle microphysics, cloud processes, and inorganic heterogeneous chemistry) are imbedded within the meteorological model's physics package, this component in turn is imbedded within the meteorological model's dynamics package, which also handles chemical tracer advection. A detailed description of the process representation of GEM-MACH, and an evaluation of its performance for pollutants such as ozone and particulate matter (PM) appears in Moran et al. (2013); Makar et al. (2015a, b); Gong et al. (2015).

GEM-MACH is used operationally to issue twice-daily, 48-hour public forecasts of criteria air pollutants (ozone, nitrogen oxides, PM), as well as the the Air Quality Health Index [<https://ec.gc.ca/cas-aqhi/>]. Any improvements to  $\text{NH}_3$  in the model may result in better AQHI predictions, since  $\text{NH}_3$  is a major precursor of  $\text{PM}_{2.5}$ , as mentioned in the introduction. We start with a similar, research version of GEM-MACHv2 to make the bidirectional flux modifications. The key differences between this and older versions are the use of a more recent meteorological package (GEMv4.8), the capability to nest in the vertical dimension as well as the horizontal dimension, and improvements to the treatment of fluxes, vertical diffusion, and advection.

GEM-MACH can be run for many different spatial domains, at various spatial resolutions, and in 2-bin or 12-bin aerosol size distribution modes. For this study we run the model in the 2-bin mode (for computational efficiency), using a nested set of domains. The outer domain at 10-km resolution covers North America, and the inner domain at 2.5-km resolution covers the provinces of Alberta and Saskatchewan. The latter is referred to as the 2.5-km Oil Sands domain. This set up, along with the emissions described in the next section is hereafter called our "base" simulation.

## 2.1 Emissions

The emissions of 25 species ( $\text{SO}_2$ ,  $\text{SO}_4$  (gas), sulphate, nitrate,  $\text{NH}_4^+$ , NO,  $\text{NO}_2$ ,  $\text{NH}_3$ , CO, nitrous acid, benzene, propane, higher alkanes, higher alkenes, ethene, toluene, aromatics, formaldehyde, aldehydes, methyl ethyl ketone, creosol, isoprene, crustal material, elemental carbon, and primary carbon) used in GEM-MACH (base case) come from Canadian and U.S. emissions inventories: 2011 National Emissions Inventory (NEI) version 1 for U.S. emissions, and the Air Pollutant Emission Inventory (APEI) 2013 for Canadian emissions (2010 for onroad and offroad emissions). Emissions were processed with SMOKE (Sparse Matrix Operator Kernel Emissions, <https://www.cmascenter.org/smoke/>) to convert the inventories into model-ready gridded hourly emissions files for modeling, separated into major point emissions (typically industrial emissions from stacks, emitted into the model layers that correspond to the stack height, at the reported temperature and velocity in the inventory's stack parameters), and area emissions (emissions from spread-out sources, such as transportation and agriculture, emitted into the first model layer). For more details about these emissions, see Moran et al. (2015) and Zhang et al. (2017, this issue).

The emissions data for  $\text{NH}_3$  from oil sands sources are reported to the Canadian National Pollutant Release Inventory (NPRI) on a "total annual emissions per facility" basis.  $\text{NH}_3$  emissions are generally more uncertain than  $\text{SO}_2$  and  $\text{NO}_x$  emissions because  $\text{NH}_3$  emissions are not measured to the same extent as those two. The oil sands represent only 1% of total Alberta  $\text{NH}_3$  emissions, at approximately 1438 tonnes in 2013. For comparison, about  $18\times$  more  $\text{NO}_x$  and  $57\times$  more  $\text{SO}_2$  was emitted from the oil sands facilities that year (<http://www.ec.gc.ca/inrp-npri/donnees-data/index.cfm?lang=En>). However, we found an issue with  $\text{NH}_3$  in this inventory that impacted our model evaluation in the region, which we describe below. The emissions data for  $\text{NH}_3$  from oil sands sources are reported to the Canadian National Pollutant Release Inventory (NPRI) on a "total annual emissions per facility" basis.  $\text{NH}_3$  emissions are generally more uncertain than  $\text{SO}_2$  and  $\text{NO}_x$  emissions because  $\text{NH}_3$  emissions are not measured to the same extent as those two. The oil sands represent only 1% of total Alberta  $\text{NH}_3$  emissions, at approximately 1438 tonnes in 2013. For comparison, about  $18\times$  more  $\text{NO}_x$  and  $57\times$  more  $\text{SO}_2$  was emitted from the oil sands facilities that year (<http://www.ec.gc.ca/inrp-npri/donnees-data/index.cfm?lang=En>). However, we found an issue with  $\text{NH}_3$  in this inventory that impacted our model evaluation in the region, which we describe below.

If stack parameters (e.g., stack height and diameter, volume flow rates, temperatures, etc.) are included as part of that data, then the emissions are allocated to large stacks in our configuration of the SMOKE emissions processing system. In the absence of this information, SMOKE will assign default stack parameters based on its source category code. For the Syncrude Canada Ltd. - Mildred Lake Plant Site, NPRI ID 2274 (a facility in the AOSR), the default stack parameters were: 18.90 m for the stack height (which is within the first model layer), 0.24 m for the stack diameter, 320.0 K for the exhaust temperature, and 0.58 m/s for the exhaust velocity. However, when these defaults were applied in initial model simulations, they were found to result in erroneous short term plume

165 events with simulated surface NH<sub>3</sub> levels up to 2 orders of magnitude higher than ground observa-  
 tions, and modelled concentrations aloft too low compared to aircraft measurements (see Section 3).  
 Conversely, for species such as SO<sub>2</sub>, for which stack parameters were reported, the model was able  
 to correctly place the SO<sub>2</sub> enhancements in space and time, relative to observations. When the stack  
 parameters of the main stack for this facility were used for NH<sub>3</sub> emissions as well (stack height=183  
 170 m, stack diameter=7.9 m, exit temperature=513 K, exit velocity=23.9 m/s, from the NPRI website),  
 the simulation of surface NH<sub>3</sub> was greatly improved. All subsequent simulations reported here make  
 use of this correction.

## 2.2 Ammonia bidirectional flux parameterization

NH<sub>3</sub> can be both deposited from the atmosphere to the ground, and re-emitted from soils and plants  
 175 back to the atmosphere. The two taken together are called bidirectional flux, since the flux of NH<sub>3</sub>  
 can go both up and down. The source of NH<sub>3</sub> available for re-emissions are from the accumulated  
 NH<sub>x</sub> in the soil and stomatal water, which can arise from increased deposition from anthropogenic  
 sources, as well as from organic nitrogen decomposition (Booth et al., 2005), N<sub>2</sub>-fixation (Vile et al.,  
 2014), and natural microbial action (McCalley and Sparks, 2008).

180 The bidirectional flux scheme of Zhang et al. (2010) was applied within the GEM-MACHv2  
 model, replacing the original deposition velocity for NH<sub>3</sub> only (deposition velocity of other gas  
 species follows a scheme based on a multiple resistance approach and a single-layer “big leaf” ap-  
 proach (Wesely, 1989; Zhang et al., 2002; Robichaud and Lin, 1991; Robichaud, 1994)). The bidi-  
 rectional flux scheme is described in detail in Zhang et al. (2010), but we summarize it here.

185 Bidirectional exchange occurs between air-soil and air-stomata interfaces. The bidirectional flux  
 ( $F_t$ ) equation is:

$$F_t = -\frac{C_a - C_c}{R_a + R_b} \quad (1)$$

where  $R_a$  and  $R_b$  are the aerodynamic and quasi-laminar resistances, respectively.  $C_a$  is the NH<sub>3</sub>  
 concentration in the air, and  $C_c$  is the canopy compensation point concentration, given by Eq. (2).

$$190 \quad C_c = \frac{\frac{C_a}{R_a + R_b} + \frac{C_{st}}{R_{st}} + \frac{C_g}{R_{ac} + R_g}}{(\frac{C_a}{R_a + R_b})^{-1} + (\frac{C_{st}}{R_{st}})^{-1} + (\frac{C_g}{R_{ac} + R_g})^{-1} + (\frac{C_{cut}}{R_{cut}})^{-1}} \quad (2)$$

where  $C_{st}$  and  $C_g$  are the stomatal and ground compensation points, and  $R_i$  are the resistances in  
 s/m of the ground/soil ( $R_g$ ), stomata ( $R_{st}$ ), cuticle ( $R_{cut}$ ), and in-canopy aerodynamic ( $R_{ac}$ ). All  
 resistance formulas can be found in Zhang et al. (2003).

Stomata (st) and ground (g) compensation points are both calculated using Eq. (3):

$$195 \quad C_{st,g} = \frac{A}{T_{st,g}} \exp\left(\frac{-B}{T_{st,g}}\right) \Gamma_{st,g} \quad (3)$$

$A$  and  $B$  are constants derived from the equilibria constants for NH<sub>3</sub>(g) in leaves’ stomatal cavities to  
 NH<sub>4</sub><sup>+</sup> and OH<sup>-</sup> in the water contained in the apoplast within the leaf and in the soil where NH<sub>3</sub>(g) in

the soil pore air space is in equilibrium with the  $\text{NH}_4^+$  and  $\text{OH}^-$  dissolved in soil water (Pleim et al., 2013).  $A=161500$  mol K/L (Nemitz et al., 2000), or  $2.7457 \times 10^{15}$  ugK/m<sup>3</sup> (Pleim et al., 2013) for  
 200  $\text{NH}_3$  for both stomata and soil.  $B=10380$  (Nemitz et al., 2000).  $\Gamma_{st,g}$  is the emission potential of the stomata and ground, respectively and, in theory, is equal to the  $\text{NH}_4^+$  concentration over the  $\text{H}^+$  concentration in the apoplast water of the canopy leaves or soil water:

$$\Gamma_{st,g} = \frac{[\text{NH}_4^+]_{st,g}}{[\text{H}^+]_{st,g}} \quad (4)$$

However, since there are no modeled  $\text{NH}_4^+$  and  $\text{H}^+$  apoplast water concentrations to use, we use  $\Gamma_{st,g}$   
 205 from Wen et al. (2014), which are based on long-term empirical averages. Wen et al. (2014) gives a range of values for emission potentials for 26 land use categories (LUCs), and we use the low-end of the values in our model with the following exceptions: We further lower the  $\Gamma_g$  for agriculture LUCs to 800, and increase  $\Gamma_{st}$  of boreal forest LUCs to 3000, all of which were necessary in order to achieve realistic  $\text{NH}_3$  concentrations (e.g., compared to reported AMoN values), while staying  
 210 consistent with  $\Gamma$  findings from the literature.

This version of the model, which we call GEM-MACH-Bidi (or just "bidi" hereafter) was quite sensitive to the selection of emission potentials, which are themselves highly uncertain (Wen et al., 2014). GEM-MACH-Bidi uses the exact same emissions as in the base case, described in the previous section. However, when the sign of  $F_t$  in Eq. (1) becomes positive (that is, when  $C_a < C_c$ ),  
 215 the bidirectional flux acts effectively as an additional source of  $\text{NH}_3$  gas, releasing stored  $\text{NH}_3$  until and unless the ambient concentration rises to the compensation point concentration. When the flux is negative, net deposition of  $\text{NH}_3$  occurs.

It is important to note that  $C_{st,g}$  values are exponentially dependent on temperature (Fig. 1 shows an example of this relationship for the dominant LUCs in the northern part of the domain), and the  
 220 higher the compensation point is, the greater the likelihood there will be upward flux. The lower  $C_{st,g}$  is, the more likely there will be deposition. Since our simulation occurred in August and September 2013, when the average temperature in the AOSR was about 18°C ([agriculture.alberta.ca/acis/alberta-weather-data-viewer.jsp](http://agriculture.alberta.ca/acis/alberta-weather-data-viewer.jsp)), we expect to have more  $\text{NH}_3$  re-emission than at other times of the year. During the rest of the year (e.g., the preceding winter and spring), the compensation point would be much lower, greatly increasing the likelihood to have net deposition, even in northern Alberta/Saskatchewan where  
 225 ambient  $\text{NH}_3$  concentrations are low. Other meteorological factors affect the magnitude of bidirectional via the resistance terms. For example canopy compensation points have been observed to decrease with decreasing wind velocity, and increased precipitation (Flechard and Fowler, 1998; Fowler et al., 1998; Biswas et al., 2005; Zhang et al., 2010). In other words, we expect more re-emission during  
 230 higher winds and drier conditions.

Other chemical transport models, such as GEOS-Chem and CMAQ use a similar method as Zhang et al. (2010), however, instead of the constant average soil emission potentials used here, they utilize a CMAQ-agroecosystem coupled simulation to calculate a soil pool from which to esti-

mate  $\Gamma_g$  (Bash et al., 2013; Pleim et al., 2013; Zhu et al., 2015). In this case, the emission potential  
235 will vary and can go to zero if the  $\text{NH}_4^+$  in the pool is depleted. However, it was shown in Wen et al.  
(2014) that their  $\Gamma_{st,g}$  worked well during the same time of year as this investigation (August and  
September). This time of year was also shown in Zhu et al. (2015) to not have a large effect on emis-  
sions from the  $\text{NH}_4^+$  pool. Additionally, Wentworth et al. (2014) calculated the approximate relative  
240 abundances of  $\text{NH}_x$  in the boundary layer versus  $\text{NH}_4^+$  in the soil pool to assess whether surface-to-  
air fluxes were sustainable. They found that soil  $\text{NH}_4^+$  were much greater than boundary layer  $\text{NH}_x$   
(by over two orders of magnitude), further supporting the assumption made here. In addition, the  
turnover time for soil  $\text{NH}_4^+$  is on the order of one day, hence it is unlikely that  $\text{NH}_3$  bi-directional  
fluxes would significantly deplete/enhance soil  $\text{NH}_4^+$  pools. Finally, given that GEM-MACH is used  
for real-time air quality forecasts at Environment and Climate Change Canada, it is not desirable for  
245 our bidirectional flux scheme to have to rely in advance on another model's output. Therefore, we  
use this simplified version, and assess whether its results provide an improvement (smaller biases  
and better correlations to measurements) to simulated  $\text{NH}_3$  for less cost in run time.

### 2.3 Addition of forest fire emissions

Our third model scenario (called "fire+bidi" hereafter) uses the GEM-MACH-Bidi model, and the  
250 exact same area emissions and anthropogenic major point emissions as the base and bidi sce-  
narios. However, in addition, we add hourly North American forest fire emissions for all species  
to the major point emissions. The forest fire emissions system for GEM-MACH (called "Fire-  
work") is described in detail in Pavlovic et al. (2016). Briefly, to calculate the fire emissions for  
input to FireWork, biomass burning areas are first identified in near real time by the Canadian  
255 Wildland Fire Information System (CWFIS), which is operated by the Canadian Forest Service  
(<http://cwfis.cfs.nrcan.gc.ca/home>). CWFIS uses fire hotspots detected by NASA's Moderate Resolu-  
tion Imaging Spectroradiometer (MODIS) and NOAA's Advanced Very High Resolution Radiometer  
(NOAA/AVHRR) and Visible Infrared Imaging Radiometer Suite (VIIRS) imagery as inputs. Daily  
total emissions per hotspot are then estimated by the Fire Emission Production Simulator (FEPS)  
260 module of the BlueSky Modeling Framework (Larkin et al., 2009). SMOKE was then used to pre-  
pare model-ready hourly emissions of several species (including  $\text{NH}_3$ ) in a point-source format for  
model input.

In Environment and Climate Change Canada's operational forest fire forecasts, these emissions are  
used at 10-km resolution for the domain encompassing North America, with forest fires being treated  
265 as point sources with specific plume rise (Pavlovic et al., 2016). We have added 2013 forest fire  
emissions which were originally created for the 2013 Firework forecasts to the anthropogenic point  
source emissions used in the base case simulation, and modified the GEM-MACH model to be able  
to accommodate the changing number of major point sources each day (as the fires are parametrized  
as major points, and their number changes daily). Fire plume rise is an ongoing area of investigation

270 (e.g., Heilman et al., 2014; Paugam et al., 2016); smoldering emissions tend to be emitted directly at  
the surface, whereas flaming emissions can inject plumes to the upper troposphere. Here, we have set  
all fire emissions to be distributed evenly throughout the boundary layer, which is a simplification,  
but one that averages out smoldering and flaming plume heights. Different parameterizations of  
fire plume rise are currently under development in GEM-MACH. The Fireworks fire emissions are  
275 described in detail in Zhang et al., (2017, this issue), and this study represents the first time they have  
been used at a 2.5-km horizontal resolution.

#### 2.4 Model setup for three scenarios

The base, bidi, and fire+bidi models were all run with the following input files: Analysis files, which  
are the products of meteorological data assimilation and provide optimized initial conditions for  
280 the 12 UTC hour of each day, were obtained from ECCO archives (Buehner et al., 2013, 2015;  
Caron et al., 2015), and the numerical weather prediction regional GEM model was run regionally  
at 10-km and the high resolution GEM model was run at 2.5-km resolution to produce meteorological  
files to drive the model simulation. The base, bidi, and fire+bidi scenarios were run from 1 August to  
7 September, 2013, where the first 11 days were “spin up” in order to allow chemical concentrations  
285 to stabilize, and are not used in our evaluation. This is a sufficient amount of spinup time, given that  
the atmospheric lifetime of  $\text{NH}_3$  is typically up to 1 day (Seinfeld and Pandis, 1998; Aneja et al.,  
2001), and given that it is close to the transport time of air crossing the larger North American  
domain. The time period from 12 August to 7 September was chosen to coincide with the intensive  
measurement campaign described in Section 3.

290 The model was run in a nested setup, whereby the North American domain was run at 10-km  
resolution using “climatological” chemical initial and boundary conditions from a 1-year MOZART  
simulation for all pollutants (Giordano et al., 2015). The nested Oil Sands region (which covers most  
of Alberta and Saskatchewan) was run at 2.5-km horizontal resolution, using the initial and boundary  
conditions from the 10-km North American model run. Figure 2 shows the two model domains.

295 The model simulations for the pilot and nested domains were not run as a continuous multiday  
forecast, but rather following to the operational air quality forecast process, where the meteorolog-  
ical values are updated regularly with new analyses, in order to prevent chaotic drift of the model  
meteorology from observations. Consequently, our simulation setup comprises simulations on the  
North American domain in 30-hour cycles starting at 12 UTC, and the Oil Sands domain in 24-hour  
300 cycles starting at 18 UTC (the 6 hour lag being required to allow meteorological spinup of the lower  
resolution model). The next cycle uses the chemical concentrations from the end of the last cycle as  
initial conditions for the next 24-30 hours. This system of staggered meteorological driving forecasts  
with a continuous concentration record continues until the full time period completes.

We run GEM-MACH in the 2-bin particle mode, which means that particles fall in either fine  
305 mode (diameter 0-2.5  $\mu\text{m}$ ) or coarse mode (diameter 2.5-10  $\mu\text{m}$ ), for computational efficiency (al-

though sub-binning is used in some particle microphysics processes in order to ensure an accurate representation of particle microphysics (Moran et al., 2010)), and in order to follow the setup used for the operational 10-km resolution GEM-MACH forecast.

### 3 Measurements

310 Our three model simulations (base, bidi, and fire+bidi) are evaluated with surface, aircraft, and Cross-track Infrared Sounder (CrIS) satellite measurements. We briefly describe each of these observations below.

#### 3.1 AMS13 ground measurements

An extensive suite of instrumentation was deployed at monitoring site AMS13 (57.1492°N, 111.6422°W, 315 270 m.a.s.l., Fig. 3) from 7 August 2013 until 12 September 2013. Mining operations and bitumen upgrading facilities are 5 km to the south and north of the site. It is surrounded by boreal forest, with dominant winds from the west, averaging 1.9 m/s throughout the year. The average temperatures in the region for August are highs in the low 20s°C, and lows around 10°C, which is warm enough to make upward NH<sub>3</sub> flux more likely (recall Fig. 1), but temperatures 320 drop rapidly at the end of August, into September, where the September highs average around 15°C, lows around 5°C. The skies are the clearest during August, with at least partly clear skies 50% of the time. That said, the warm season (May through September) is the wetter season (20% chance daily average), with more precipitation than during the cold season (7% chance daily average), but year round precipitation, as well as relative humidity are both relatively low in the 325 AOSR. During the cold season (November through February), the average temperatures range from -21°C to -5°C, when the forest and soils are more likely to be a deposition sink for NH<sub>3</sub>. During November to April, it is also much cloudier, with February having cloudy conditions 77% of the time. (All weather data cited here are from the annual report at Fort McMurray, found here: <https://weatherspark.com/y/2795/Average-Weather-in-Fort-McMurray-Canada-Year-Round>).

330 NH<sub>3</sub>, fine particulate ammonium and nitrate, and other species were measured by the Ambient Ion Monitor-Ion Chromatograph (AIM-IC), via an inlet 4.55 m off the ground. The uncertainty of these measurements is ± 15%. These measurements are described in more detail in Markovic et al. (2012).

Data gaps sometimes appeared in the surface NH<sub>3</sub> time series for the following reasons: instrument zero (Aug 14/15 and 17/18), instrument maintenance (Aug 19) and a power outage (Aug 335 27/28).

### 3.2 Aircraft measurements

During the Oil Sands Monitoring Intensive campaign, there were a total of 22 flights spanning 13 August to 7 September 2013. These measurements are described in detail in Shephard et al. (2015);  
340 Gordon et al. (2015); Liggio et al. (2016); Li et al. (2017), and are summarized here. Aircraft  $\text{NH}_3$   
measurements were conducted with a dual quantum cascade laser (QCL) trace gas monitor (Aerodyne Inc., Billerica, MA, USA; McManus et al., 2008), collecting data every 1 s. Outside air was sampled through a heated Teflon inlet tube shared with a high-resolution time-of-flight chemical ionization mass spectrometer (HR-ToF-CIMS); the flow rate through the QCL was  $10.8 \text{ L min}^{-1}$ .  
345 The  $1 \sigma$  uncertainty for each measurement is estimated to be  $\pm 0.3 \text{ ppbv}$  ( $\pm 35\%$ ) (Shephard et al., 2015).

Particulate  $\text{NH}_4^+$  and  $\text{NO}_3^-$  ( $0 < 1 \mu\text{m}$  in diameter) were measured by the Aerodyne high-resolution time-of-flight aerosol mass spectrometer (HR-ToF-AMS) instrument on board the same flights, which collected data every 10 s. The ambient air was drawn through a forward facing, shrouded  
350 isokinetic particle inlet from which the HR-ToF-AMS sub-sampled. The total residence time in the inlet and associated tubing was approximately 1 second. The error on these measurements is  $\pm 9\%$ . (Liggio et al., 2016)

Figure 3 shows a sample flight path from the campaign from 13 August 2013 – one of the thirteen flights with valid  $\text{NH}_3$  measurements. The others took place on 15-17, 19 (two this day), 22-24,  
355 26, 28 August, and 5-6 September 2013.  $\text{NH}_3$  data on the other nine flights were invalidated due to instrument issues (those on 14, 20-21, 29, 31 August, and 2-4 September 2013), but were successful for the  $\text{NH}_4^+$  and  $\text{NO}_3^-$  measurements.

### 3.3 CrIS satellite measurements

CrIS was launched in late October 2011 on board the Suomi NPP platform. CrIS follows a sun-synchronous orbit with a daytime overpass time at 13:30 (ascending) and a night time equator overpass at 1:30 (descending), local time. The instrument scans along a 2200 km swath using a  $3 \times 3$   
360 array of circular pixels with a diameter of 14 km at nadir for each pixel. The CrIS Fast Physical Retrieval (CFPR) described by Shephard and Cady-Pereira (2015) is used to perform satellite profile retrievals of ammonia volume mixing ratio (VMR) given the infrared emission spectrum from the atmosphere. This retrieval uses an optimal estimation approach (Rogers, 2000) that provides the  
365 satellite vertical sensitivity (averaging kernels) and an estimate of the total errors (error covariance matrix).

We take the CrIS retrieved profile and match it up with the closest model profile in both distance and time, compute the distance between the CrIS pixel and model field for each time step, and then  
370 select the time step that best matches the satellite overpass time. Since the model time steps are

every hour with a 10-km spatial resolution they are always matched up to better than half an hour, and within 5 km.

## 4 Model evaluation

An older version of GEM-MACH (v1.5.1) has been compared to TES satellite and aircraft measurements of ammonia over the AOSR (Shephard et al., 2015). Simulations with that version of the model were shown to be biased low, by about -0.5 ppbv, throughout the lower-tropospheric vertical profile. This represented a substantial deficit in the model predicted sources of  $\text{NH}_3$ , prompting the current work. We now compare our three GEM-MACH simulations (base, bidi, and fire+bidi) against surface point measurements at the measurement site near an oil sands facility (AMS13), aircraft measurements over the broader AOSR, and satellite measurements over the Alberta and Saskatchewan area. We will discuss which simulation agrees best with measurements and where there may still be room for additional model improvement.

### 4.1 At the AMS13 ground site

Figure 4 shows the timeseries of the daily average (for clarity) concentrations of  $\text{NH}_3$  and fine-particulate  $\text{NH}_4^+$ ,  $\text{NO}_3^-$ , and  $\text{SO}_4^{2-}$  at the AMS13 Oil Sands ground site for the observations and three model simulations. The hourly data were also studied, but not shown in the time series.

We first note that the  $\text{NH}_3$  concentrations seen in the measured time series are relatively low with mean, median, and maximum of 0.6 ppbv, 0.426 ppbv, and 2.98 ppbv, respectively in the hourly data, which are lower than the 1-8 ppbv range in Bytnerowicz et al. (2010), and the 2.7 ppbv summertime mean given in Hsu and Clair (2016). However, this may be due to the different time periods and locations measured. Our mean measured values at the AMS13 site are similar to the concentrations found at U.S. AMoN background sites (<http://nadp.sws.uiuc.edu/amon/>).

Figure 4a shows that the base model (green) background concentrations of  $\text{NH}_3$  are very low (nearly 0 ppbv when there is no plume influence) compared to the measurements (orange). Only during the spike on September 3-4th does the base model exceed the measured values, probably indicating a local plume event fumigating to a lesser extent in the observations than was assumed in the model. The  $\text{NH}_3$  concentrations of the base case are biased low compared to the surface measurements by a median of -0.35 ppbv (Fig. 5a) over the time period of the campaign – comparable to the bias observed in satellite observations in Shephard et al. (2015). In Figure 4, the bidi model (blue line) and fire+bidi model (red line) show a significant improvement to the  $\text{NH}_3$  concentrations compared to the base model (green line). Unfortunately, during some time periods, these two versions of the model overestimate  $\text{NH}_3$ : During August 13th, the model adds a significant level of  $\text{NH}_3$  due to fire emissions, however the surface *in situ* observations show no evidence of fire impact. During other time periods (e.g., 30 August to 3 September, and 4-7 September), the bidi model appears to

405 have put too much  $\text{NH}_3$  into the system. Therefore, the bidi model bias (Fig. 5a) is now 0.30 ppbv too high (median), and the fire+bidi bias is 0.32 ppbv high (median) over the time period of the campaign, resulting in an overall improvement of only 0.03 ppbv in the model bias.

While the bias improvement is small, the bidi and fire+bidi both have greatly improved correlation coefficients (from  $R=0.1$  to  $0.4$ ) and slopes much closer to 1 (from  $0.1$  to  $0.7$ ), showing that those  
410 added sources are important to improve model results (Fig. 6a). Additionally, the diurnal cycle (not shown) was improved in the bidi simulation, with both it and the measurements shaped like a sine curve having a minimum at 3:00-4:00am local time, and a maximum at noon local time, although the amplitude of the cycle was underestimated. Whereas, the base model diurnal cycle was flat from midnight to noon local time, and spikey from noon to midnight.

415 While Fig. 4a to 6a show that the addition of bidirectional flux significantly improves the model correlation coefficient, slope, and bias, there is still room for improvement. Paired t-test results indicate that the fire+bidi and measurements are still significantly different (see Table 2 for comparison statistics of all three simulations). While inherent limitations from model resolution and uncertainties may be responsible for the remaining bias, it is likely that (a) the emission potentials for the  
420 land use categories (LUCs) in the region may be causing too much re-emission of  $\text{NH}_3$ , and need refinement, and (b) the fire emissions of  $\text{NH}_3$  are not properly distributed in the vertical, placing too much  $\text{NH}_3$  near the surface and/or the fire emission factors for  $\text{NH}_3$  are too high.

Refinement needed for the emission potentials and LUCs may be a significant cause of the bidi and fire+bidi model biases. Rooney et al. (2012) have shown that about 64% of the AOSR are wet-  
425 lands (fens, bogs and marshes), which should be mapped to the swamp LUC. However, our model currently assigns the AOSR landscape to evergreen needleleaf trees, deciduous broadleaf trees, inland lake, mixed shrubs, and mixed forests (and none of the region to swamp). This would lead to an overestimation of re-emission given that bogs are fairly acidic and our swamp emission potential is lower than the aforementioned LUCs. Other evidence for these two explanations will be presented  
430 below in Section 4.3.

The time series, model-vs-measured correlations, and model biases of  $\text{NH}_4^+$ ,  $\text{NO}_3^-$ , and  $\text{SO}_4^{2-}$  are also shown in Fig. 4 to 6 (b, c, and d, respectively). For  $\text{NH}_4^+$  and  $\text{SO}_4^{2-}$  there is very little change despite the increase in  $\text{NH}_3$  that the bidirectional flux yields. The bias is very small for all three model scenarios, and the correlation coefficients are all relatively poor. So while there is an  
435 improvement to modelled  $\text{NH}_3$  with bidirectional flux, there is a neutral affect on fine particulate  $\text{NH}_4^+$ . This may be because the charge of  $\text{NH}_4^+$  in the particles is already enough in the base model to balance the charge of  $2 \times \text{SO}_4^{2-} + \text{NO}_3^-$  in the aerosols, thus, causing any additional  $\text{NH}_3$  (from bidi and fires) to remain in the gas phase. Or it could be due to additional wet scavenging of the additional ammonium, which will be discussed in Section 5.2. The change in  $\text{NH}_3$  concentrations  
440 has no effect on  $\text{SO}_4^{2-}$  since particulate  $\text{SO}_4^{2-}$  is not sensitive to the amount of  $\text{NH}_3/\text{NH}_4^+$  available, and is dominated by anthropogenic and fire emissions. For  $\text{NO}_3^-$ , the base model bias was quite

small at  $0.01 \mu\text{m}/\text{m}^3$ , however the addition of bidi and fire+bidi further reduced that bias to 0.0011 and  $0.0004 \mu\text{m}/\text{m}^3$ , respectively, which is a significant improvement. The correlation coefficient for  $\text{NO}_3^-$  also improved from about 0.1 to 0.3 (Fig. 6c).

#### 445 4.2 Along the OS campaign flight paths

There were 13 flights during the OS campaign that had valid (above detection limit, and no instrument error)  $\text{NH}_3$  measurements, and 22 flights that had valid  $\text{NH}_4^+$  ( $0-1 \mu\text{m}$  diameter) measurements. The flight path of the first flight, which occurred on 13 August 2013 is shown in Fig. 3; chosen as an example because this flight sampled mainly background  $\text{NH}_3$  concentrations (rather than facility  
450 plumes).

Figure 7 shows the  $\text{NH}_3$  concentrations along this flight path over time. Here the hourly model output is interpolated to the same time frequency as the measurements. The model also has spatial resolution limits when comparing to the aircraft. However, we clearly see that for this flight, the bidirectional flux has increased  $\text{NH}_3$  concentrations, bringing them closer to the measured values  
455 (median biases for this flight are -1.38, 0.68, and 0.69 ppbv in the base, bidi, and fire+bidi simulations). There is little change when fires are added (Fig 7d vs c) because this flight did not pass through a fire plume.

Figure 8 shows the model-measurement differences and the model vs measurement scatter plots for the combined set of all flight paths for hourly-average concentrations of  $\text{NH}_3$  and  $\text{NH}_4^+$ . For  $\text{NH}_3$   
460 the median base model bias is -0.75 ppbv, comparable to the bias observed in Shephard et al., 2015, with the bidi model bias improving to -0.24 ppbv, and the fire+bidi bias to -0.23 ppbv. Also the best correlation coefficient and slope is achieved by the fire+bidi scenario. The use of the bidirectional flux has thus reduced the model bias relative to the aircraft observations by a factor of three. The fire+bidi simulation has the best statistics compared to measurements, as summarized in Table 2.

465 Again, the  $\text{NH}_4^+$  results show little change despite the increase in  $\text{NH}_3$  concentrations. The small bias from the base case gets insignificantly smaller, and the slope and correlation coefficients are all negligibly changed.

#### 4.3 In the vertical profiles across the region

The CrIS satellite has many observations over North America during the 2013 Oil Sands campaign.  
470 We have evaluated the model with these observations in a number of ways:

1. All daytime data from Aug 12 - September 7th, 2013; model-measurement comparisons over a large region encompassing Alberta and Saskatchewan, latitude range:  $48-60^\circ\text{N}$ , longitude range:  $100-122^\circ\text{W}$ , which contains agricultural areas, a number of cities, the northern boreal forest, and the Oil Sands facilities.

475 2. Case studies where we attempt to isolate fire emissions and non-fire conditions to evaluate  
both new components (fires and bidi) of the model.

The latitude and longitude ranges of our model-measurement pairs are given in Table 1. The satellite passes over these regions at approximately 1pm and 1am local time.

There were over 60 000 model-measurement pairs between the model and the CrIS satellite over  
480 the model domain during August 12th to September 7th, 2013. Figure 9top panel presents model  
biases for the entire dataset in a box and whiskers plot of the vertical  $\text{NH}_3$  profiles at five vertical lev-  
els. The left-most panel shows the  $\text{NH}_3$  concentrations measured by CrIS, and the right-most panel  
shows the diagonal elements of the CrIS averaging kernels, illustrating the sensitivity of the satellite  
measurements to each vertical level. The  $\text{NH}_3$  concentrations over Alberta and Saskatchewan mea-  
485 sured by CrIS are very similiar to those found by TES in the Shephard et al. (2015) study for the  
AOSR region.

The middle panels show the model biases from the three simulations. The fire+bidi model has the  
smallest bias in the highest three layers, but the bidi model has the smallest bias in the two low-  
est layers, whereas the fire+bidi model increases  $\text{NH}_3$  concentrations further (though still a smaller  
490 absolute bias compared to the base case, Fig. 9top). This could be due to an overestimate of the bidi-  
rectional flux re-emissions or of the fire emissions, or to an underestimate of the altitude of the fire  
emissions, or a combination of all three factors. In order to distinguish between these possibilities,  
two case studies were examined further below. The statistics from the model-CrIS comparison can  
be found in Table 2. That summary shows that the fire+bidi simulation performs better than the base  
495 and the bidi simulations.

The spatial distribution of modelled  $\text{NH}_3$  can also be evaluated with CrIS measurements, as shown  
in the bottom panel of Figure 9. These are maps of the average surface  $\text{NH}_3$  concentrations from  
the base model, the fire+bidi model, and the CrIS satellite. The fire+bidi model over-predicts the  
effect of fires in the middle of northern Saskatchewan, but appears to be missing fires in north-  
500 western Manitoba. Other than fire influence, the spatial distribution in the fire+bidi model is the same  
as that of the base model, but with significant increases in overall concentrations. And the spatial  
distribution of the model simulations is different from the spatial distribution that CrIS measures.  
For example, the model predicts much higher  $\text{NH}_3$  concentrations near the city of Edmonton than  
CrIS shows. That said, the addition of bidirectional flux has greatly improved the  $\text{NH}_3$  concentrations  
505 in the northern part of the province, where there was almost none in the base model.

We selected three sample days (3 Sept, 1 Sept and 12 Aug, 2013) that we use for the case stud-  
ies, and surface  $\text{NH}_3$  concentrations over that region as well as sample Aqua MODIS true colour  
composite maps for those days are shown (Fig. 10). The four boxed regions on those maps indicate  
where model-measurement pairs were sampled for this study. The cyan and black boxes in Fig. 10a  
510 and b are the regions where we sample clear-sky, no-fire conditions on 3 and 1 September 2013,  
respectively. The magenta box in Fig. 10c is the region where we isolated our fire case study on 12

August 2013. The blue box is the region we discussed above, which we analysed for the full time period simulated (12 Aug - 7 Sep 2013, Fig. 9top).

#### 4.3.1 Case study 1: clear-sky days with little fire influence - evaluating bidi

515 In order to evaluate the bidirectional flux component separately from the fire component, we selected September 1st (southern, agricultural region - black box in Fig. 10b), and 3rd (northern, boreal forest and AOSR region - cyan box in Fig. 10a), where the MODIS map (EOSDIS NASA World view map, [worldview.earthdata.nasa.gov](http://worldview.earthdata.nasa.gov)) shows very little hot spots from fires, and that the conditions were relatively cloud and smoke free (which yield the most CrIS observations). See Table 1 for the latitude and longitude ranges. Figure 10 also shows the surface  $\text{NH}_3$  concentrations as observed by CrIS on each of those days. Figure 11a shows that in the north, the bidi model improves the bias from -0.84 ppbv to -0.07 ppbv in the lowest vertical level, and smaller, but still significant, improvements to the bias at the other levels. The fire+bidi model has a nearly identical impact as the bidi model, which is expected in a fire-free zone. Therefore, the GEM-MACH-Bidi model performs very well in northern Alberta and Saskatchewan where there is mainly boreal forest, and background-level  $\text{NH}_3$  concentrations. This also implies that the LUC assignment discussed in Section 4.1 may only apply to a small region around the AOSR, and not to the overall large region we've defined here.

In the southern region (Fig. 11b), the addition of bidirectional flux moves the bias from near-zero to +1.02 ppbv in the lowest level. In this case, the base model with no bidirectional flux appears to be the most accurate model in areas dominated by agricultural sources. There are two possible explanations: a) agricultural emissions are too high in the base model, and the addition of the bidirectional flux leads to an overestimation of the  $\text{NH}_3$  amounts, or b) re-emissions from bidirectional flux from crops are not significant. The literature (Bash et al., 2010; Massad et al., 2010; Zhang et al., 2010; Zhu et al., 2015) indicate that crops do indeed re-emit  $\text{NH}_3$ , therefore, (a) is the more likely explanation. The agriculture  $\text{NH}_3$  emission inventory we used was created by the NAESI (National Agri-Environmental Standards Initiative) project (Bittman et al., 2008; Ayres et al., 2009; Makar et al., 2009) have about 30-200% uncertainty associated with them (Bouwman et al., 1997; Asman et al., 1998). Therefore, with improved national  $\text{NH}_3$  emission inventories, the GEM-MACH-Bidi should improve model results across the domain.

#### 540 4.3.2 Case study 2: a clear day with significant fire influence - evaluating fires

In order to evaluate the fire component separately from the bidirectional flux, we selected August 12th (a northern region with little-to-no agricultural contributions) where the MODIS map shows numerous hot spots from fires and smokey conditions (Fig. 10c, magenta box). The base and bidi models underestimate  $\text{NH}_3$  concentrations (Fig. 11c) by -6.22 and -5.84 ppbv, respectively (in the lowest vertical layer), but the fire+bidi model overestimates  $\text{NH}_3$  by +4.06 ppbv. The fire+bidi version of the model still has the lowest bias of the three simulations, however, either (a) the fire+bidi

model does not distribute the fire emissions properly in the vertical, (b) the fire emissions of  $\text{NH}_3$  are too high, and/or (c) the model is not properly representing  $\text{NO}_2$  and  $\text{SO}_2$  in the fire, and so the conversion of  $\text{NH}_3$  to  $\text{NH}_4^+$  is underestimated. It is potentially a combination of all three explanations, and we further elaborate below.

– For explanation (a), both fire plume rise and fire emission factors are on-going areas of study. In the model the fire emissions are distributed evenly throughout the boundary layer (the first 3-4 layers in Fig. 11c), however, Shinozuka et al. (2011) suggest that sometimes the fire plumes are distributed normally in a thin layer aloft. However, should that be the case for the real-life fires in this case study, the model bias would be negative at at least one of the levels in Fig. 11c, which it is not. Figure 11c shows that the positive bias extends throughout the first three vertical layers, and in the top two vertical layers, the bias does not move further negative (as would happen in the fire plume were actually at those altitudes in real life).

– (a) Our bias would be very high at low levels if the real fire plumes were actually above 4 km (above the altitudes we studied), however, it was found that the plume heights for most of the Fort McMurray fires of 2016 reached only up to 3-4 km altitude range based on the NASA Cloud-Aerosol Lidar and Infrared Pathfinder Satellite Observation (CALIPSO) and Multi-angle Imaging SpectroRadiometer (MISR) satellite observations. Therefore, this is not likely the case.

– Explanation (b) seems the most likely, as the uncertainty on emission factors for  $\text{NH}_3$  from wildfires is very large (e.g., 50-100% depending on the fuel type Urbanski, 2014), and could easily be overestimated.

– The  $\text{NO}_x$  and  $\text{SO}_2$  fire emission factors (c) have smaller uncertainties of 10-40% (Urbanski, 2014).

Unfortunately, there were no flights that captured the fine structure of the fire plumes during the 2013 monitoring intensive campaign that can be used to further corroborate the vertical distribution of the fire plumes. There will however be flight observations of fires during the planned 2018 AOSR measurement campaign. Therefore, the model may be further improved with reduced  $\text{NH}_3$  emission factors for fires, and/or improved vertical distribution of fire plumes.

## 5 Impacts of bidirectional flux and forest fires on $\text{NH}_3$ concentrations

### 5.1 Effect on ambient concentrations

Given that the overall fire+bidi model agrees best with measurements in the greater Alberta/Saskatchewan region (discussed throughout Section 4) and contains all known missing sources of  $\text{NH}_3$ , we can use the model to answer one of our key questions: What percent contributions to total ambient  $\text{NH}_3$

580 concentrations came from bidirectional flux and from forest fires during the study time period? We do so by subtracting the bidi model output from the fire+bidi model output to get the forest fire component, and subtracting the base model output from the bidi model output to get the bidi component. The absolute differences are calculated as follows:

$$bidi\ component = NH_3^{bidi} - NH_3^{base} \quad (5)$$

585

$$fire\ component = NH_3^{fire+bidi} - NH_3^{bidi}, \quad (6)$$

which tell us how many ppbv of  $NH_3$  on average comes from re-emissions of  $NH_3$  (upward component of bidirectional flux), and from fire emissions.

The percent differences are calculated as follows:

$$590 \quad bidi\ percent = \frac{NH_3^{bidi} - NH_3^{base}}{NH_3^{fire+bidi}} \times 100\% \quad (7)$$

$$fire\ percent = \frac{NH_3^{fire+bidi} - NH_3^{bidi}}{NH_3^{fire+bidi}} \times 100\%, \quad (8)$$

which tell us what percent of total  $NH_3$  concentrations on average comes from re-emissions of  $NH_3$  (upward component of bidirectional flux), and from fire emissions, assuming the  $NH_3$  from our  
595 fire+bidi simulation is the true total  $NH_3$ .

We perform this calculation on the averaged model output (12 August to 7 September 2013) over the 2.5-km model domain, and get an average of 20.3% (or 0.42 ppbv) and a median of 10.4% for ambient surface  $NH_3$  concentrations that come from forest fires (Fig. 12). The mean and median are so different because fires are sporadic, large contributions to  $NH_3$  concentrations, and the mean  
600 value is more sensitive to the big outliers. We get an average of 56.6% (or 1.24 ppbv) from bidirectional flux (56.3%, median), and the remaining 23.1%, average (33.3 %, median) comes from direct emissions from anthropogenic sources (agriculture, fossil fuel combustion, oil sands industry, etc). These numbers are summarized in Table 3. The increase in  $NH_3$  concentrations due to the bidirectional flux scheme is of the same order of magnitude as that found in the Zhu et al. (2015) study  
605 using the GEOS-Chem model, during the month of July, in the United States (where they found 1 ppbv increase in surface concentrations due to bidirectional flux). It is also similar to values found in Europe in the Wichink Kruit et al. (2010) study.

Over the model domain, the minimum bidi influence on surface  $NH_3$  is just north of Edmonton, where only 1% of  $NH_3$  comes from bidi. Similarly, two AOSR facilities north of Fort McMurray  
610 stand out as having small bidi influence (12-40 %, surrounded by values in the 90s% - Fig. 12d). Also, any remote region with fire emissions will have a small percentage contribution from bidirectional flux during the fires, as they are in northern Saskatchewan (Fig. 12d). This is expected given that the average concentrations in cities and near large sources are very close to, or exceed the compensation point. The absolute maximum in the bidi component map is 4.5 ppbv in the lower right

615 corner (an agricultural region with high  $\text{NH}_3$  emissions), and the minimum is 0 ppbv (Fig. 12b). This means that nowhere in the domain, did the bidirectional flux formula result in more net deposition than the base model calculated via the Welesley/Robichaud/Zhang scheme. The maximum fire contribution to surface  $\text{NH}_3$  is 27.9 ppbv where large fires occurred in northern Saskatchewan (Fig. 12c).

## 620 5.2 Effect on Deposition

Similar to our analysis from the previous section, we can use the model to determine how bidirectional flux and fires impact daily  $\text{NH}_x$  deposition (which equals the dry deposition of  $\text{NH}_3$  + the wet deposition of  $\text{NH}_4^+$ ). Figure 13 shows the average daily net deposition (or net flux) of  $\text{NH}_x$  from the base, bidi, and fire+bidi models. Negative (or blue) indicates net deposition (downward flux), and positive (or red), net emission (upward flux). The base model (Fig. 13a) had no re-emission (upward flux) option, thus  $\text{NH}_3$  was always net dry deposited in that scenario. The bidi (Fig. 13b) and fire+bidi (Fig. 13c) maps show that most of the Alberta and Saskatchewan area has net deposition (e.g., near the cities, agriculture, and forest fires), but that some regions (with low atmospheric  $\text{NH}_3$  concentrations) have net emission of  $\text{NH}_x$ . The dry  $\text{NH}_3$  flux is net positive over the domain, however, when the increase in wet  $\text{NH}_4^+$  is accounted for, the net flux of  $\text{NH}_x$  is still negative (downward). This is very similar to what Wichink Kruit et al. (2010) found in a 2007 study in Europe; a reduction in dry  $\text{NH}_3$ , compensated by an increase wet  $\text{NH}_4^+$  deposition.

Note that the assumption of an infinite soil pool of  $\text{NH}_4^+$  in our bidirectional flux scheme has not caused an overwhelming upward flux of  $\text{NH}_x$ . In fact, the average results across the domain actually have more deposition in the fire+bidi scenario than in our base scenario. Table 4 shows the mean and median net  $\text{NH}_x$  flux for each scenario (presented as deposition, so negative signs removed). That said, following the soil pool approach (Pleim et al., 2013; Zhu et al., 2015), the soil pool of  $\text{NH}_4^+$  may eventually get depleted. However, that is very unlikely for the following reasons: (1) Deposition of  $\text{NH}_x$  throughout the year continually replenishes the soil pool – especially when temperatures are cooler in winter, spring, and fall, since the compensation point is exponentially dependent on temperature. (2) The short time frame of this study would not be long enough to deplete the soil pool. For example, Zhu et al. (2015) needed to spin up their model for three months in order to get the  $\text{NH}_4$  soil pool stable.

In the AOSR near Fort McMurray, we can compare our  $\text{NH}_3$  dry deposition results to those calculated in Hsu and Clair (2015). Their values range from 0.7 to 1.25 kg-N/ha/year (or  $1.13$  to  $2.01 \times 10^{-5}$  moles/m<sup>2</sup>/day), and ours are 10 times lower at around 0.13 kg-N/ha/year (or  $2.12 \times 10^{-6}$  moles/m<sup>2</sup>/day) near Fort McMurray, and do not vary much among our three model scenarios. Our deposition underestimate may be partially due to the fact that our modelled ambient  $\text{NH}_3$  concentrations are also low compared to those measured in Hsu and Clair (2016) near Fort McMurray. They measured an average of  $1.55 \pm 0.6$  ppbv ( $1.9 \mu\text{g}/\text{m}^3$ ) at Fort McMurray, whereas our fire+bidi model

has an average of 1.01 ppbv there (0.73 ppbv in bidi, and 0.39 in base). There may also be differences in that our model has more of the  $\text{NH}_x$  deposition coming down as  $\text{NH}_4^+$ , rather than as  $\text{NH}_3$ .

Our fire+bidi  $\text{NH}_x$  deposition values (Table 4) are well in line with reported  $\text{NH}_3$  deposition in Kharol et al. (2017), who report satellite-derived  $\text{NH}_3$  deposition of about  $2.1\text{--}7.0 \times 10^{-5}$  moles/m<sup>2</sup>/day in Alberta), and are at the low end of  $\text{NH}_3$  deposition values reported within Behera et al. (2013).

The difference in deposition between the fire+bidi and bidi cases – which is the contribution of fires to the total  $\text{NH}_x$  flux – showed that the fires increased downward flux/deposition over large swaths of the domain (e.g., difference between Figure 13c and b). The fires contributed an average of  $1.954 \times 10^{-5}$  moles/m<sup>2</sup>/day of  $\text{NH}_x$  deposition across the domain.

While the particulate  $\text{NH}_4^+$  concentrations did not change much in our three simulations (see Sections 4.1 and 4.2), the wet deposition of  $\text{NH}_4^+$  increased significantly going from the base to bidi to fire+bidi models. This is in contrast to what Zhu et al. (2015) found, which was little change to  $\text{NH}_4^+$  due to bidirectional flux. However that could be due other parameters, such as the meteorological conditions, scavenging parameters, and/or gas-particle partitioning of  $\text{NH}_x$ . It would seem that in GEM-MACH-Bidi, the increased  $\text{NH}_3$  concentrations were scavenged by precipitation. The average  $\text{NH}_4^+$  deposition from the three simulations had a nearly threefold increase in the  $\text{NH}_4^+$  deposition due to the increased  $\text{NH}_3$  concentrations that the fire+bidi simulation yields. The average  $\text{NH}_4^+$  wet deposition for our fire+bidi simulation is  $5.86 \times 10^{-5}$  moles/m<sup>2</sup>/day, which is in between values reported in the United States in Stensland et al. (2000) (where they found an average of  $1.9 \times 10^{-5}$  moles/m<sup>2</sup>/day over the country), and in Japan in Murano et al. (1998) (where they found an average of  $10.3 \times 10^{-5}$  moles/m<sup>2</sup>/day over the country).

In the three scenarios, the average daily relative ratio of dry/wet deposition was: 0.43 for base, -0.77 for bidi, and -0.51 for fire+bidi (the negative value for the bidi and fire+bidi cases are because of the average upward direction of  $\text{NH}_3$ ). Since all average ratios are less than 1, this means that most of the removal process is from wet deposition, rather than dry deposition (even for the base case that had no re-emission of  $\text{NH}_3$ ). Therefore, increased monitoring of wet deposition in the region would be useful. These results may also be useful for AEP terrestrial/aquatic scientists interested in nitrogen eutrophication. Maps of these ratios can be found in the supplemental material.

## 6 Conclusions

The GEM-MACHv2 air quality forecasting model was altered to include both the Zhang et al. (2010) bidirectional flux scheme for  $\text{NH}_3$  and forest fire emissions of all species. This new “fire+bidi” model greatly improves the simulated  $\text{NH}_3$  in the modelled Oil Sands domain at 2.5-km resolution when compared to independent *in situ* measurements at the ground (at the AMS13 oil sands monitoring site) and aloft (aircraft measurements), as well as at 10-km resolution when compared to cutting-edge satellite measurements from the CrIS instrument. Almost all comparison statistics are best with

our fire+bidi simulation. This suggests that the fire+bidi model shows promise for improving NH<sub>3</sub> model predictions elsewhere and during other time periods. However, more work is required to validate the model in other regions of the continent (e.g., with the Wood Buffalo Environmental Association (WBEA) and the U.S. Ammonia Monitoring Network (AMoN) surface networks, and further  
690 CrIS satellite measurements), and for different time periods (e.g., springtime fertilizer season, cooler conditions, etc.). We have also shown that for further improvements in the Alberta/Saskatchewan region, the NH<sub>3</sub> emission factors for fires, and the NH<sub>3</sub> emissions from agriculture likely need to be reduced.

Despite the significant increase in NH<sub>3</sub> concentrations with these additional sources, the impact  
695 on its byproduct, NH<sub>4</sub><sup>+</sup>, was miniscule - as was the change to SO<sub>4</sub><sup>2-</sup> concentrations (0.02 μg/m<sup>3</sup> for each). The model bias for those species was not significantly changed in either direction. This is probably because of the extra NH<sub>4</sub><sup>+</sup> wet scavenging by precipitation, and the NH<sub>3</sub> concentrations were already high enough (before adding the extra sources) to charge balance the SO<sub>4</sub><sup>2-</sup> and NO<sub>3</sub><sup>-</sup> in the aerosols. Thus, any additional NH<sub>3</sub> would remain in the gas phase. That said, the model bias for  
700 NO<sub>3</sub><sup>-</sup> at the AMS13 ground station was essentially removed with the fire+bidi model.

By running the base, bidi, and fire+bidi model scenarios, and taking the fire+bidi results as “true”, we were able to calculate their differences and determine the average contributions from each source. We found that, on average, during the 12 August to 7 September 2013 time period in the Alberta/Saskatchewan model domain, 23.1% of surface NH<sub>3</sub> comes from direct anthropogenic  
705 emissions, 56.6% of surface NH<sub>3</sub> comes from bidirectional flux (re-emission from soils and plants), and 20.3% of NH<sub>3</sub> comes from forest fires. Possible sources of error that remain in the bidi and fire+bidi simulations are the agricultural and fire emissions of NH<sub>3</sub>, as well as the emission potentials for different land-use categories. The fraction of NH<sub>3</sub> from fires is highly variable depending on the time periods and spatial domain analysed: on average from 12 August to 7 September 2013,  
710 the largest impact was in northern Saskatchewan. We expect the re-emission source to be near the highest at this time of year because of the high temperatures, and this source should be much lower during the cold season, when deposition is expected to dominate the bidirectional flux process.

The bidirectional flux process has decreased NH<sub>x</sub> deposition on average across the domain, with some areas having a net emission of NH<sub>3</sub>. However, that upward flux is due to the low atmospheric  
715 concentrations and high temperatures, and does not exceed the amount of NH<sub>x</sub> deposition that occurs during the cooler winter and spring times. When fires are also taken into account, the net NH<sub>x</sub> deposition is greater, on average across the domain, compared to the base model.

*Acknowledgements.* The project was supported by Environment and Climate Change Canada’s Oil Sands Monitoring program (OSM), and the Climate Change and Air Quality Program (CCAP). We would also like to  
720 acknowledge the University of Wisconsin-Madison Space Science and Engineering Center Atmosphere SIPS

team sponsored under NASA contract NNG15HZ38C for providing us with the CrIS level 1 and 2 input data, in particular Keven Hrpcek and Liam Gumley.

Data availability: The CrIS-FRP-NH<sub>3</sub> science data products used in this study can be made available on request (M. W. Shephard, Environment and Climate Change Canada, Toronto, Ontario, Canada). Similarly, the  
725 AMS13 observations can be made available on request from Greg Wentworth (AEP), and the model output or code from Cynthia Whaley (ECCC). The aircraft observations are on the ECCC data portal (<http://donnees.ec.gc.ca/data/air/monitor/ambient-air-quali>)

## References

- Aneja, V., Bunton, B., Walker, J., and Malik, B.: Measurement and analysis of atmospheric ammonia emissions from anaerobic lagoons, *Atmos. Environ.*, 35, 1949 – 1958, 730 doi:[https://doi.org/10.1016/S1352-2310\(00\)00547-1](https://doi.org/10.1016/S1352-2310(00)00547-1), 2001.
- Asman, W. A. H., Sutton, M. A., and Schjorring, J. K.: Ammonia: emission, atmospheric transport and deposition, *New Phytologist*, 139, 27–48, doi:10.1046/j.1469-8137.1998.00180.x, 1998.
- Ayres, J., Bittman, S., Girdhar, S., Sheppard, S., Niemi, D., Ratte, D., and Smith, P.: Chapter 5: Sources of Ammonia Emissions, in: *The 2008 Canadian Atmospheric Assessment of Agricultural Ammonia*, Environment and Climate Change Canada, Gatineau, QC, Canada, 2009. 735
- Bash, J. O., Walker, J. T., Katul, G. G., Jones, M. R., Nemitz, E., and Robarge, W. P.: Estimation of In-Canopy Ammonia sources and sinks in a fertilized *Zea mays* field, *Environ. Sci. Tech.*, 44, 1683–1689, doi:10.1021/es9037269, 2010.
- Bash, J. O., Cooter, E. J., Dennis, R. L., Walker, J. T., and Pleim, J. E.: Evaluation of a regional air-quality 740 model with bidirectional NH<sub>3</sub> exchange coupled to an agroecosystem model, *Biogeosciences*, 10, 1635–1645, doi:10.5194/bg-10-1635-2013, 2013.
- Beer, R., Shephard, M. W., Kulawik, S. S., Clough, S. A., Eldering, A., Bowman, K. W., Sander, S. P., Fisher, B. M., Payne, V. H., Luo, M., Osterman, G. B., and Worden, J. R.: First satellite observations of lower tropospheric ammonia and methanol, *Geophys. Res. Lett.*, 35, doi:10.1029/2008GL033642, 109801, 2008.
- 745 Behera, S. N., Sharma, M., Aneja, V. P., and Balasubramanian, R.: Ammonia in the atmosphere: a review on emission sources, atmospheric chemistry and deposition on terrestrial bodies, *Environ. Sci. Pollut. Res. Int.*, 20, 8092–8131, doi:10.1007/s11356-013-2051-9, 2013.
- Biswas, H., Catterjee, A., Mukhopadhyaya, S. K., De, T. K., Sen, S., and Jana, T. K.: Estimation of ammonia exchange at the land ocean boundary condition of Sundarban mangrove, northeast coast of Bay of Bengal, 750 *India, Atmos. Environ.*, 39, 4489–4499, doi:10.1016/j.atmosenv.2005.03.041, 2005.
- Bittman, S., Ayres, J., S. Sheppard, S., and Girdhar, S.: Chapter 4: Emission Inventory Development, in: *The 2008 Canadian Atmospheric Assessment of Agricultural Ammonia*, Environment and Climate Change Canada, Gatineau, QC, Canada, 2008.
- Booth, M. S., Stark, J. M., and Rastetter, E.: Controls on nitrogen cycling in terrestrial ecosystems: a synthetic 755 analysis of literature data, *Ecol. Monogr.*, 75, 139–157, 2005.
- Bouwman, A., Lee, D. S., Asman, W. A. H., Dentener, F. J., van der Hoek, K. W., and Olivier, J. G. J.: A global high-resolution emission inventory for ammonia, *Glob. Biogeochem. Cycles*, 11, 561–587, doi:10.1029/97GB02266, 1997.
- Buehner, M., Morneau, J., and Charette, C.: Four-dimensional ensemble-variational data assimilation for global deterministic weather prediction, *Nonlinear Processes Geophys.*, 20, 669–682, 760 doi:10.5194/npg-20-669-2013, 2013.
- Buehner, M., McTaggart-Cowan, R., Beaulne, A., Charette, C., Garand, L., Heilliette, S., Lapalme, E., Laroche, S. S. R. M., Morneau, J., and Zadra, A.: Implementation of Deterministic Weather Forecasting Systems based on Ensemble-Variational Data Assimilation at Environment Canada. Part I: The Global System, *Mon. Wea.* 765 *Rev.*, 143, 2532–2559, doi:10.1175/MWR-D-14-00354.1, 2015.

- Bytnerowicz, A., Fraczek, W., Schilling, S., and Alexander, D.: Spatial and temporal distribution of ambient nitric acid and ammonia in the Athabasca Oil Sands Region, Alberta, *J. Limnol.*, 69, 11–21, doi:10.3274/JL10-69-S1-03, 2010.
- 770 Carfrae, J. A., Sheppard, L. J., Raven, J., Stein, W., Leith, I. D., Theobald, A., and Crossley, A.: Early effects of atmospheric ammonia deposition on *Calluna vulgaris* (L.) hull growing on an ombrotrophic peat bog, *Water Air Soil Pollut. Focus*, 4, 229–239, doi:10.1007/s11267-004-3033-1, 2004.
- Caron, J.-F., Milewski, T., Buehner, M., Fillion, L., Reszka, M., Macpherson, S., and St-James, J.: Implementation of deterministic weather forecasting systems based on ensemble–variational data assimilation at Environment Canada. Part II: The regional system, *Mon. Wea. Rev.*, 143, 2560–2580, 775 doi:10.1175/MWR-D-14-00353.1, 2015.
- Charpentier, A. D., Bergerson, J. A., and McLean, H. L.: Understanding the Canadian oil sands industry’s greenhouse gas emissions, *Environ. Res. Lett.*, 4, 1–11, doi:10.1088/1748-9326/4/1/014005, 2009.
- 780 Ciais, P., Sabine, C., Bala, G., Bopp, L., Brovkin, V., Canadell, J., Chhabra, A., DeFries, R., Galloway, J., Heimann, M., Jones, C., Le Quéré, C., Myneni, R. B., Piao, S., and Thornton, P.: Carbon and Other Biogeochemical Cycles, in: *Climate Change 2013: The Physical Science Basis, Contribution of Working Group I to the Fifth Assessment Report of the Intergovernmental Panel on Climate Change*, edited by Stocker, T. F., Qin, D., Plattner, G.-K., Tignor, M., Allen, S. K., Boschung, J., Nauels, A., Xia, Y., Bex, V., and Midgley, P. M., p. 465–570, Cambridge University Press, Cambridge, United Kingdom and New York, NY, USA, 2013.
- 785 Clair, T. A. and Percy, K. E.: *Assessing forest health in the Athabasca Oil Sands Region*, Wbea technical report, Wood Buffalo Environmental Agency, Alberta, 2015.
- Clarisse, L., Clerbaux, C., Dentener, F., Hurtmans, D., and Coheur, P.-F.: Global ammonia distribution derived from infrared satellite observations, *Nature Geosci.*, 2, doi:10.1038/ngeo551, 109801, 2009.
- 790 Dragosits, U., Theobald, M., Place, C., Lord, E., Webb, J., Hill, J., ApSimon, H., and Sutton, M.: Ammonia emission, deposition and impact assessment at the field scale: a case study of sub-grid spatial variability, *Environmental Pollution*, 117, 147 – 158, doi:https://doi.org/10.1016/S0269-7491(01)00147-6, 2002.
- Ellis, R., Murphy, J. G., Markovic, M. Z., VandenBoer, T. C., Makar, P. A., Brooks, J., and Mihele, C.: The influence of gas-particle partitioning and surface-atmosphere exchange on ammonia during BAQS-Met, *Atmos. Chem. Phys.*, 11, 133–145, doi:10.5194/acp-11-133-2011, 2011.
- 795 Environment and Climate Change Canada: *Canadian Environmental Sustainability Indicators: Air Pollutant Emissions*, Technical report, Environment and Climate Change Canada, ECCC Public Inquiries Centre, 200 Sacre-Coeur boul. Gatineau, QC, K1A 0H3, <http://www.ec.gc.ca/indicateurs-indicators/default.asp?lang=en&n=E79F4C12-1>, 2016.
- 800 Environment and Climate Change Canada: *Criteria air contaminants*, Tech. rep., Environment and Climate Change Canada and Canadian Council of Ministers of the Environment, <https://www.ec.gc.ca/air/default.asp?lang=En&n=7C43740B-1>, last referenced 9 June 2017, 2017.
- Environment Canada: *Precursor contributions to ambient fine particulate matter in Canada*, Report, Air Quality Research Division, Environment and Climate Change Canada, Toronto, Ontario, Canada, 2001.

- Fangmeier, A., Hadwiger-Fangmeier, A., der Eerden, L. V., and Jäger, H.-J.: Effects of atmospheric ammonia on vegetation—A review, *Environmental Pollution*, 86, 43 – 82, doi:[http://dx.doi.org/10.1016/0269-7491\(94\)90008-6](http://dx.doi.org/10.1016/0269-7491(94)90008-6), 1994.
- Farquhar, G. D., Firth, P. M., Wetselaar, R., and Weir, B.: On the Gaseous Exchange of Ammonia between Leaves and the Environment Determination of the Ammonia Compensation Point, *Plant Physiol.*, 66, 710–714, doi:10.1104/pp.66.4.710, 1980.
- 810 Flechard, C. R. and Fowler, D.: Atmospheric ammonia at a moorland site. II: Long term surface atmosphere micrometeorological flux measurements, *Q. J. Roy. Meteor. Soc.*, 124, 759–791, doi:10.1002/qj.49712454706, 1998.
- Fowler, D., Flechard, C. R., Sutton, M. A., and Storeton-West, R. L.: Long term measurements of the land atmosphere exchange of ammonia over moorland, *Atmos. Environ.*, 32, 453–459, 815 doi:10.1016/S1352-2310(97)00044-7, 1998.
- Fu, X., Wang, S. X., Rau, L. M., Pleim, J. E., Cooter, E., Bash, J. O., Benson, V., and Hao, J. M.: Estimating NH<sub>3</sub> emissions from agricultural fertilizer application in China using the bi-directional CMAQ model coupled to an agro-ecosystem model, *Atmos. Chem. Phys.*, 15, 6637–6649, doi:10.5194/acp-15-6637-2015, 2015.
- Galloway, J. N., Townsend, A. R., Erisman, J. W., Bekunda, M., Cai, Z. C., Freney, J. R., Martinelli, L. A., 820 Seitzinger, S. P., and Sutton, M. A.: Transformation of the nitrogen cycle: Recent trends, questions, and potential solutions, *Science*, 320, 889–892, doi:10.1126/Science.1136674, 2008.
- Galperin, M. and Sofiev, M.: The long-range transport of ammonia and ammonium in the Northern Hemisphere, *Atmos. Environ.*, 32, 373 – 380, doi:10.1016/S1352-2310(97)00045-9, 1998.
- Giordano, L., Brunner, D., Flemming, J., Hogrefe, C., Im, U., Bianconi, R., Badia, A., Balzarini, A., Baró, 825 R., Chemel, C., Curci, G., Forkel, R., Jiménez-Guerrero, P., Hirtl, M., Hodzic, A., Honzak, L., Jorba, O., Knote, C., Kuenen, J., Makar, P., Manders-Groot, A., Neal, L., Pérez, J., Pirovano, G., Pouliot, G., José, R. S., Savage, N., Schröder, W., Sokhi, R., Syrakov, D., Torian, A., Tuccella, P., Werhahn, J., Wolke, R., Yahya, K., Zabkar, R., Zhang, Y., and Galmarini, S.: Assessment of the MACC reanalysis and its influence as chemical boundary conditions for regional air quality modeling in AQMEII-2, *Atmos. Environ.*, 115, 830 371–388, doi:10.1016/j.atmosenv.2015.02.034, 2015.
- Gong, W., Makar, P. A., Zhang, J., Milbrandt, J., Gravel, S., Hayden, K. L., Macdonald, A. M., and Leitch, W. R.: Modelling aerosol cloud meteorology interaction: A case study with a fully coupled air quality model GEM-MACH, *Atmos. Environ.*, 115, 695–715, doi:10.1016/j.atmosenv.2015.05.062, 2015.
- Gordon, M., Li, S.-M., Staebler, R., Darlington, A., Hayden, K., O'Brien, J., and Wolde, M.: Determining air 835 pollutant emission rates based on mass balance using airborne measurement data over the Alberta oil sands operations, *Atmos. Meas. Tech.*, 8, 3745–3765, doi:10.5194/amt-8-3745-2015, 2015.
- Hansen, K., Personne, E., Skjoth, C. A., Loubet, B., Ibrom, A., Jensen, R., Sorensen, L. L., and Boegh, E.: Investigating sources of measured forest-atmosphere ammonia fluxes using two-layer bi-directional modelling, *Agriculture and Forest Meteorology*, 237-238, 20–94, doi:10.1016/j.agrformet.2017.02.008, 2017.
- 840 Heilman, W. E., Liu, Y., Urbanski, S., Kovalev, V., and Mickler, R.: Wildland fire emissions, carbon, and climate: Plume rise, atmospheric transport, and chemistry processes, *Forest Ecology and Management*, 317, 70 – 79, doi:<http://dx.doi.org/10.1016/j.foreco.2013.02.001>, wildland fire emissions, carbon, and climate: Science overview and knowledge needs, 2014.

- Hsu, Y.-M. and Clair, T. A.: Measurement of fine particulate matter water-soluble inorganic species and precursor gases in the Alberta Oil Sands Region using an improved semicontinuous monitor, *J. Air Waste Manage. Assoc.*, 65, 423–435, doi:10.1080/10962247.2014.1001088, 2015.
- Hsu, Y.-M. and Clair, T. A.: Measurement of fine particulate matter water-soluble inorganic species and precursor gases in the Alberta Oil Sands Region using an improved semicontinuous monitor, *J. Air Waste Manage. Assoc.*, 568, 285–295, doi:10.1016/j.scitotenv.2016.05.205, 2016.
- 850 IPCC: Climate Change 2013: The Physical Science Basis, Contribution of Working Group I to the Fifth Assessment Report of the Intergovernmental Panel on Climate Change, in: IPCC Fifth Assessment Report, edited by Stocker, T. F., Qin, D., Plattner, G.-K., Tignor, M., Allen, S. K., Boschung, J., Nauels, A., Xia, Y., Bex, V., and Midgley, P. M., Cambridge University Press, Cambridge, United Kingdom and New York, NY, USA, 2013.
- 855 Jimenez, J. L., Canagaratna, M. R., Donahue, N. M., and et al: Evolution of Organic Aerosols in the Atmosphere, *Science*, 326, 1525–1529, doi:10.1126/science.1180353, 2009.
- Kelly, E. N., Short, J. W., Schindler, D. W., Hodson, P. V., Ma, M., Kwan, A. K., and Fortin, B. L.: Oil sands development contributes polycyclic aromatic compounds to the Athabasca River and its tributaries, *Proc. Natl. Acad. Sci.*, 106, 22 346–22 351, doi:10.1073/pnas.0912050106, 2009.
- 860 Kharol, S. K., Shephard, M. W., McLinden, C. A., Zhang, L., Sioris, C. E., O'Brien, J. M., Vet, R., Cady-Pereira, K. E., Hare, E., Siemons, J., and Krotkov, N. A.: Dry deposition of reactive nitrogen from satellite observations of ammonia and nitrogen dioxide over North America, *Geophys. Res. Lett.*, doi:10.1002/2017GL075832, 2017.
- Kirk, J. L., Muir, D. C. G., Gleason, A., Wang, X., Lawson, G., Frank, R. A., Lehnher, I., and Wrona, F.: Atmospheric Deposition of Mercury and Methylmercury to Landscapes and Waterbodies of the Athabasca Oil Sands Region, *Environ. Sci. Technol.*, 48, 7374–7383, doi:10.1021/es500986r, 2014.
- 865 Krupa, S.: Effects of atmospheric ammonia (NH<sub>3</sub>) on terrestrial vegetation: a review, *Environmental Pollution*, 124, 179 – 221, doi:10.1016/S0269-7491(02)00434-7, 2003.
- Lamarque, J.-F., Bond, T. C., Eyring, V., Granier, C., Heil, A., Klimont, Z., Lee, D., Liousse, C., Mieville, A., Owen, B., Schultz, M. G., Shindell, D., Smith, S. J., Stehfest, E., Van Aardenne, J., Cooper, O. R., Kainuma, M., Mahowald, N., Mc-Connell, J. R., Naik, V., Riahi, K., and van Vuuren, D. P.: Historical (1850–2000) gridded anthropogenic and biomass burning emissions of reactive gases and aerosols: methodology and application, *Atmos. Chem. Phys.*, 10, 7017–7039, doi:10.5194/acp-10-7017-2010, 2010.
- 870 Larkin, N. K., O'Neill, S. M., Solomon, R., Raffuse, S., Strand, T., Sullivan, D., Krull, C., Rorig, M., Peterson, J., and Ferguson, S. A.: The BlueSky smoke modeling framework, *Int. J. Wildland Fire*, 18, 906–920, doi:10.1071/WF07086, 2009.
- Lee, C. J., Martin, R. V., Henze, D. K., Brauer, M., Cohen, A., and van Donkelaar, A.: Response of Global particulate matter related mortality to changes in local precursor emissions, *Environ. Sci. and Tech.*, 49, 4335–4344, doi:10.1021/acs.est.5b00873, 2015.
- 880 Li, S.-M., Leithead, A., Moussa, S. G., Liggio, J., Moran, M. D., Wang, D., Hayden, K., Darlington, A., Gordon, M., Staebler, R., Makar, P. A., Stroud, C. A., McLaren, R., Liu, P. S. K., O'Brien, J., Mittermeier, R. L., Zhang, J., Marson, G., Cober, S. G., Wolde, M., and Wentzell, J. J. B.: Differences between measured and

- reported volatile organic compound emissions from oil sands facilities in Alberta, Canada, *Proc. Nat. Acad. Sci.*, doi:10.1073/pnas.1617862114, 2017.
- 885 Liggio, J., Li, S.-M., Hayden, K., Taha, Y. M., Stroud, C., Darlington, A., Drollette, B. D., Gordon, M., Lee, P., Liu, P., Leithead, A., Moussa, S. G., Wang, D., O'Brien, J., Mittermeier, R. L., Brook, J. R., Lu, G., Staebler, R. M., Han, Y., Tokarek, T. W., Osthoff, H. D., Makar, P. A., Zhang, J., L. Plata, D., and Gertner, D. R.: Oil sands operations as a large source of secondary organic aerosols, *Nature*, 534, 91–94, doi:10.1038/nature17646, 2016.
- 890 Makar, P., Bouchet, V. S., and Nenes, A.: Inorganic chemistry calculations using HETV - a vectorized solver for the  $\text{SO}_4^{2-}$ - $\text{NO}_3^-$ - $\text{NH}_4^+$  system based on the ISORROPIA Algorithms, *Atmos. Environ.*, 37, 2279–2294, doi:10.5194/acp-9-7183-2009, 2003.
- Makar, P., Moran, M., Zheng, Q., Cousineau, S., Sassi, M., Duhamel, A., Besner, M., Davignon, D., Crevier, L.-P., and Bouchet, V. S.: Modelling the impacts of ammonia emissions reductions on North American air quality, *Atmos. Chem. Phys.*, 9, 7183–7212, doi:10.1016/S1352-2310(03)00074-8, 2009.
- 895 Makar, P., Gong, W., Hogrefe, C., Zhang, Y., Curci, G., Zabkar, R. ., Milbrandt, J., Im, U., Balzarini, A., Baró, R., Bianconi, R., Cheung, P., Forkel, R., Gravel, S., Hirtl, M., Honzak, L., Hou, A., Jiménez-Guerrero, P., Langer, M., Moran, M., Pabla, B., Pérez, J., Pirovano, G., José, R. S., Tuccella, P., Werhahn, J., Zhang, J., and Galmarini, S.: Feedbacks between air pollution and weather, part 2: Effects on chemistry, *Atmos. Environ.*, 900 115, 499–526, doi:10.1016/j.atmosenv.2014.10.021, 2015a.
- Makar, P. A., Gong, W., Milbrandt, J., Hogrefe, C., Zhang, Y., Curci, G., Zabkar, R. ., Im, U., Balzarini, A., Baró, R., Bianconi, R., Cheung, P., Forkel, R., Gravel, S., Hirtl, M., Honzak, L., Hou, A., Jiménez-Guerrero, P., Langer, M., Moran, M., Pabla, B., Pérez, J., Pirovano, G., José, R. S., Tuccella, P., Werhahn, J., Zhang, J., and Galmarini, S.: Feedbacks between air pollution and weather, part 1: Effects on weather, *Atmos. Environ.*, 905 115, 442–469, doi:10.1016/j.atmosenv.2014.12.003, 2015b.
- Makar, P. A., Akingunola, A., Aherne, J., Cole, A. S., Aklilu, Y., Zhang, J., Wong, I., Hayden, K., Li, S. M., Kirk, J., Scott, K., Moran, M. D., Robichaud, A., Cathcart, H., Baratzehah, P., Pabla, B., Cheung, P., Zheng, Q., and Jeffries, D. S.: Estimates of exceedances of critical loads for acidifying deposition in Alberta and Saskatchewan, *Atmos. Chem. Phys. Disc.*, submitted to ACPD Oil Sands special issue, 2017.
- 910 Markovic, M. Z., VandenBoer, T. C., and Murphy, J. G.: Characterization and optimization of an online system for the simultaneous measurement of atmospheric water-soluble constituents in the gas and particle phases, *J. Env. Mon.*, 14, 1872–1884, doi:1, 2012.
- Massad, R.-S., Nemitz, E., and Sutton, M. A.: Review and parameterisation of bi-directional ammonia exchange between vegetation and the atmosphere, *Atmos. Chem. Phys.*, 10, 10359–10386, 915 doi:10.5194/acp-10-10359-2010, 2010.
- McCalley, C. K. and Sparks, J. P.: Controls over nitric oxide and ammonia emissions from Mojave Desert soils, *Oecologia*, 156, 871–881, doi:10.1007/s00442-008-1031-0, 2008.
- Moran, M., Menard, S., Gravel, S., Pavlovic, R., and Anselmo, D.: RAQDPS Versions 1.5.0 and 1.5.1: Upgrades to the CMC Operational Regional Air Quality Deterministic Prediction System Released in October 2012 and February 2013, Technical report, Canadian Meteorological Centre, Canadian Meteorological Centre, 920 Dorval, Quebec, 2013.

- Moran, M., Zheng, Q., Zhang, J., and Pavlovic, R.: RAQDPS Version 013: Upgrades to the CMC Operational Regional Air Quality Deterministic Prediction System Released in June 2015, Technical report, Canadian Meteorological Centre, Canadian Meteorological Centre, Dorval, Quebec, 2015.
- 925 Moran, M. D., Ménard, S., Talbot, D., Huang, P., Makar, P. A., Gong, W., Landry, H., Gravel, S., Gong, S., Crevier, L.-P., Kallaur, A., and Sassi, M.: Particulate-matter forecasting with GEM-MACH15, a new Canadian air-quality forecast model, in: *Air pollution modelling and its application XX*, edited by Steyn, D. G. and Rao, S. T., pp. 289–292, Springer, Dordrecht, 2010.
- Moss, R. H., Edmonds, J. A., Hibbard, K. A., Manning, M. R., Rose, S. K., van Vuuren, D. P., Carter, T. R., 930 Emori, S., Kainuma, M., Kram, T., Meehl, G. A., Mitchell, J. F. B., Nakicenovic, N., Riahi, K., Smith, S. J., Stouffer, R. J., Thomson, A. M., Weyant, J. P., and Wilbanks, T. J.: The next generation of scenarios for climate change research and assessment, *Nature*, 463, 747–756, doi:10.1038/nature08823, 2010.
- Murano, K., Mukai, H., Hatakeyama, S., Oishi, O., Utsunomiya, A., and Shimohara, T.: Wet deposition of ammonium and atmospheric distribution of ammonia and particulate ammonium in Japan, *Environmental 935 Pollution*, 102, 321 – 326, doi:10.1016/S0269-7491(98)80050-X, 1998.
- Nemitz, E., Sutton, M. A., Schjoerring, J. K., Husted, S., and Wyers, G. P.: Resistance modelling of ammonia exchange over oilseed rape, *Agr. For. Meteorol.*, 105, 405–425, doi:10.1016/S0168-1923(00)00206-9, 2000.
- Nemitz, E., Milford, C., and Sutton, M. A.: A two-layer canopy compensation point model for describing bi-directional biosphere-atmosphere exchange of ammonia, *Q. J. Roy. Meteorol. Soc.*, 127, 815–833, 940 doi:10.1002/qj.49712757306, 2001.
- Nenes, A., Pilinis, C., and Pandis, S.: ISORROPIA: A New Thermodynamic Model for Multiphase Multicomponent Inorganic Aerosols, *Aquat. Geochem.*, 4, 123–152, doi:10.1023/A:1009604003981, 1998.
- Olivier, J., Bouwman, A., der Hoek, K. V., and Berdowski, J.: Global air emission inventories for anthropogenic sources of NO<sub>x</sub>, NH<sub>3</sub> and N<sub>2</sub>O in 1990, *Environmental Pollution*, 102, 135 – 148, 945 doi:http://dx.doi.org/10.1016/S0269-7491(98)80026-2, 1998.
- Park, R. J., Jacob, D. J., Field, B. D., Yantosca, R. M., and Chin, M.: Natural and transboundary pollution influences on sulfate-nitrate-ammonium aerosols in the United States: Implications for policy, *J. Geophys. Res.*, 109, doi:10.1029/2003JD004473, d15204, 2004.
- Paugam, R., Wooster, M., Freitas, S., and Val Martin, M.: A review of approaches to estimate wildfire plume 950 injection height within large-scale atmospheric chemical transport models, *Atmos. Chem. Phys.*, 16, 907–925, doi:10.5194/acp-16-907-2016, 2016.
- Paulot, F., Jacob, D. J., Pinder, R. W., Bash, J. O., Travis, K., and Henze, D. K.: Ammonia emissions in the United States, European Union, and China derived by high-resolution inversion of ammonium wet deposition data: Interpretation with a new agricultural emissions inventory (MASAGE NH<sub>3</sub>), *J. Geophys. Res.*, 119, 955 4343–4364, doi:10.1002/2013JD021130, 2014.
- Pavlovic, R., Chen, J., Anderson, K., Moran, M., Beaulieu, P.-A., Davignon, D., and Cousineau, S.: The Fire-Work air quality forecast system with near-real-time biomass burning emissions: Recent developments and evaluation of performance for the 2015 North American wildfire season, *J. Air Waste Manage. Assoc.*, 66, 819–841, doi:10.1080/10962247.2016.1158214, 2016.

- 960 Pleim, J. E., Bash, J. O., Walker, J. T., and Cooter, E. J.: Development and evaluation of an ammonia bidirectional flux parameterization for air quality models, *J. Geophys. Res.*, 118, 3794–3806, doi:10.1002/jgrd.50262, 2013.
- Pope III, C., Burnett, R., Thun, M., and et al: Lung cancer, cardiopulmonary mortality, and long-term exposure to fine particulate air pollution, *JAMA*, 287, 1132–1141, doi:10.1001/jama.287.9.1132, 2002.
- 965 Robichaud, A.: Statistical links between meteorological factors and tropospheric ozone levels at the Duchesnay forest site, *Climat*, 12, 31–57, 1994.
- Robichaud, A. and Lin, C. A.: The linear steady response of a stratified baroclinic atmosphere to elevated diabatic forcing, *Atmosphere - Ocean*, 29, 619–635, doi:10.1080/07055900.1991.9649421, 1991.
- Rogers, C. D.: *Inverse methods for atmospheric Sounding: Theory and Practice*, World Sci., Hackensack, NJ, 970 2000.
- Rooney, R. C., Bayley, S. E., and Schindler, D. W.: Oil sands mining and reclamation cause massive loss of peatland and stored carbon, *Proc. Natl. Acad. Sci.*, 109, 4933–4937, doi:10.1073/pnas.1117693108, 2012.
- Seinfeld, J. H. and Pandis, S. N., eds.: *Atmospheric Chemistry and Physics: From Air Pollution to Climate Change*, Wiley-Intersci., New York, 1326 pp., 1998.
- 975 Shephard, M. W. and Cady-Pereira, K. E.: Cross-track Infrared Sounder (CrIS) satellite observations of tropospheric ammonia, *Atmos. Meas. Techn.*, 8, 1323–1336, doi:10.5194/amt-8-1323-2015, 2015.
- Shephard, M. W., Cady-Pereira, K. E., Luo, M., Henze, D. K., Pinder, R. W., Walker, J. T., Rinsland, C. P., Bash, J. O., Zhu, L., Payne, V. H., and Clarisse, L.: TES ammonia retrieval strategy and global observations of the spatial and seasonal variability of ammonia, *Atmos. Chem. Phys.*, 11, 10743–10763, 980 doi:10.5194/acp-11-10743-2011, 2011.
- Shephard, M. W., McLinden, C. A., Cady-Pereira, K. E., Luo, M., Moussa, S. G., Leithead, A., Liggio, J., Staebler, R. M., Akingunola, A., Makar, P., Lehr, P., Zhang, J., Henze, D. K., Millet, D. B., Bash, J. O., Zhu, L., Wells, K. C., Capps, S. L., Chaliyakunnel, S., Gordon, M., Hayden, K., Brook, J. R., Wolde, M., and Li, S.-M.: Tropospheric Emission Spectrometer (TES) satellite observations of ammonia, methanol, formic acid, 985 and carbon monoxide over the Canadian oil sands: validation and model evaluation, *Atmos. Meas. Techn.*, 8, 5189–5211, doi:10.5194/amt-8-5189-2015, 2015.
- Shinozuka, Y., Redemann, J., Livingston, J. M., Russell, P. B., Clarke, A. D., Howell, S. G., Freitag, S., O'Neill, N. T., Reid, E. A., Johnson, R., Ramachandran, S., McNaughton, C. S., Kapustin, V. N., Brekhovskikh, V., Holben, B. N., and McArthur, L. J. B.: Airborne observation of aerosol optical depth during ARC- 990 TAS: vertical profiles, inter-comparison and fine-mode fraction, *Atmos. Chem. Phys.*, 11, 3673–3688, doi:10.5194/acp-11-3673-2011, 2011.
- Stensland, G. J., Bowersox, V. C., Larson, B., and Claybrooke, R. D.: Comparison of Ammonium in USA Wet Deposition to Ammonia emission estimates, technical report, Illinois State Water Survey, 2204 Griffith Drive, Champaign, IL, 61820, <https://www3.epa.gov/ttn/chief/conference/ei10/ammonia/stensland.pdf>, 2000.
- 995 Sutton, M., Milford, C., Dragosits, U., Place, C., Singles, R., Smith, R., Pitcairn, C., Fowler, D., Hill, J., ApSimon, H., Ross, C., Hill, R., Jarvis, S., Pain, B., Phillips, V., Harrison, R., Moss, D., Webb, J., Espenhahn, S., Lee, D., Hornung, M., Ulliyett, J., Bull, K., Emmett, B., Lowe, J., and Wyers, G.: Dispersion, deposition and impacts of atmospheric ammonia: quantifying local budgets and spatial variability, *Environmental Pollution*, 102, 349 – 361, doi:http://dx.doi.org/10.1016/S0269-7491(98)80054-7, 1998.

- 1000 Sutton, M. A., Fowler, D., and Moncrieff, J. B.: The Exchange of Atmospheric Ammonia with Vegetated Surfaces .1. Unfertilized Vegetation, *Q. J. Roy. Meteorol. Soc.*, 119, 1023–1045, doi:10.1002/qj.49711951309, 1993.
- Sutton, M. A., Schjorring, J. K., and Wyers, G. P.: Plant Atmosphere Exchange of Ammonia, *Philos. T. Roy. Soc. A.*, 351, 261–276, <http://www.jstor.org/stable/54415>, 1995.
- 1005 Urbanski, S.: Wildland fire emissions, carbon, and climate: Emission factors, *Forest Ecology and Management*, 317, 51–60, doi:10.1016/j.foreco.2013.05.045, 2014.
- Van Damme, M., Clarisse, L., Heald, C. L., Hurtmans, D., Ngadi, Y., Clerbaux, C., Dolman, A. J., Erismann, J. W., and Coheur, P. F.: Global distributions, time series and error characterization of atmospheric ammonia (NH<sub>3</sub>) from IASI satellite observations, *Atmos. Chem. Phys.*, 14, 2905–2922, doi:10.5194/acp-14-2905-2014, 2014.
- 1010 Vile, M. A., Kelman Wieder, R., Živković, T., Scott, K. D., Vitt, D. H., Hartssock, J. A., Iosue, C. L., Quinn, J. C., Petix, M., Fillingim, H. M., Popma, J. M. A., Dynarski, K. A., Jackman, T. R., Albright, C. M., and Wyckoff, D. D.: N<sub>2</sub>-fixation by methanotrophs sustains carbon and nitrogen accumulation in pristine peatlands, *Biogeochemistry*, 121, 317–328, doi:10.1007/s10533-014-0019-6, 2014.
- 1015 Vitt, D. H.: Nitrogen addition experiments in boreal ecosystems: understanding the fate of atmospheric deposited nitrogen in order to determine nitrogen critical loads, Cema report, Wood Buffalo Environmental Agency, Alberta, 2016.
- Wen, D., Zhang, L., Lin, J. C., Vet, R., and Moran, M. D.: An evaluation of ambient ammonia concentrations over southern Ontario simulated with different dry deposition schemes within STILT-Chem v0.8, *Geosci. Model Dev.*, 7, 1037–1050, doi:10.5194/gmd-7-1037-2014, 2014.
- 1020 Wentworth, G. R., Murphy, J. G., Gregoire, P. K., Cheyne, C. A. L., Tevlin, A. G., and Hems, R.: Soil–atmosphere exchange of ammonia in a non-fertilized grassland: measured emission potentials and inferred fluxes, *Biogeosciences*, 11, 5675–5686, doi:10.5194/bg-11-5675-2014, 2014.
- Wesely, M. L.: Parameterization of surface resistances to gaseous dry deposition in regional-scale numerical models, *Atmos. Environ.*, 23, 1293–1304, doi:10.1016/0004-6981(89)90153-4, 1989.
- 1025 Wichink Kruit, R., van Pul, W., Sauter, F., van den Broek, M., Nemitz, E., Sutton, M., Krol, M., and Holtslag, A.: Modeling the surface–atmosphere exchange of ammonia, *Atmos. Environ.*, 44, 945 – 957, doi:10.1016/j.atmosenv.2009.11.049, 2010.
- Wieder, R. K., Vile, M. A., Albright, C. M., Scott, K. D., Vitt, D. H., Quinn, J. C., and Burke-Scoll, M.: Effects of altered atmospheric nutrient deposition from Alberta oil sands development on *Sphagnum fuscum* growth and C, N and S accumulation in peat, *Biogeochemistry*, 129, 1–19, doi:10.1007/s10533-016-0216-6, 2016a.
- 1030 Wieder, R. K., Vile, M. A., Scott, K. D., Albright, C. M., McMillen, K. J., Vitt, D. H., and Fenn, M. E.: Differential effects of high atmospheric N and S deposition on bog plant/lichen tissue and porewater chemistry across the Athabasca Oil Sands Region, *Environ. Sci. Technol.*, 50, 12 630–12 640, doi:10.1021/acs.est.6b03109, 2016b.
- 1035 Wu, Y., Walker, J., Schwede, D., Peters-Lidard, C., Dennis, R., and Robarge, W.: A new model of bi-directional ammonia exchange between the atmosphere and biosphere: Ammonia stomatal compensation point, *Agr. Forest Meteorol.*, 149, 263 – 280, doi:10.1016/j.agrformet.2008.08.012, 2009.

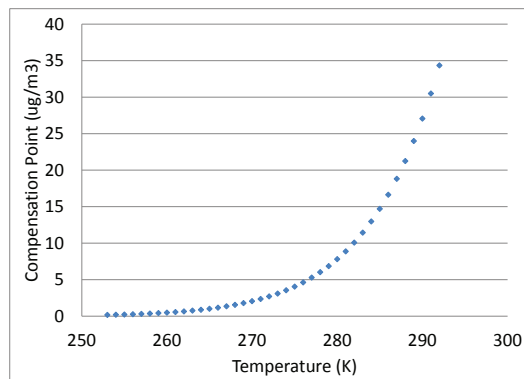


**Figure 1.** Compensation point ( $C_g$ ) relationship to temperature;  $C_g$  for evergreen needleleaf LUC shown as example.

**Table 1.** Latitude and longitude ranges that the model was evaluated over with the CrIS satellite measurements

domain	date (in 2013)	lat range (°)	lon range (°)
AB/SK large domain	12 Aug to 7 Sept	48 to 60 N	-122.0 to -100.0 W
northern, no-fire case study	3 Sept	55 to 60 N	-120.0 to -110.0 W
southern, no-fire case study	1 Sept	49 to 53.5 N	-117.0 to -106.0 W
northern, fire case study	12 Aug	56.5 to 60 N	-110.0 to -104.4 W

- Zhang, J., Moran, M. D., Zheng, Q., Makar, P. A., Baratzadeh, P., Marsen, G., Liu, P., and Li, S.-M.: Emissions preparation and analysis for multiscale air quality modelling over the Athabasca oil sands region of Alberta, Canada, *Atmos. Chem. Phys. Disc.*, submitted to ACPD Oil Sands special issue, 2017.
- 1040 Zhang, L., Moran, M., Makar, P., Brook, J., and Gong, S.: Gaseous Dry Deposition in AURAMS A Unified Regional Air-quality Modelling System, *Atmos. Environ.*, 36, 537–560, doi:10.1016/S1352-2310(01)00447-2, 2002.
- 1045 Zhang, L., Brook, J. R., and Vet, R.: A revised parametrization for gaseous dry deposition in air-quality models, *Atmos. Chem. Phys.*, 3, 2067–2082, doi:10.5194/acp-3-2067-2003, 2003.
- Zhang, L., Wright, L. P., and Asman, W. A. H.: Bi-directional air-surface exchange of atmospheric ammonia: A review of measurements and a development of a big-leaf model for applications in regional-scale air-quality models, *J. Geophys. Res.*, 115, D20 310, doi:10.1029/2009JD013589, 2010.
- 1050 Zhu, L., Henze, D. K., Cady-Pereira, K. E., Shephard, M. W., Luo, M., Pinder, R. W., Bash, J. O., and Jeong, G.-R.: Constraining U.S. ammonia emissions using TES remote sensing observations and the GEOS-Chem adjoint model, *J. Geophys. Res.*, 118, 3355–3368, doi:10.1002/jgrd.50166, 2013.
- Zhu, L., Henze, D., Bash, J., Jeong, G.-R., Cady-Pereira, K., Shephard, M., Luo, M., Paulot, F., and Capps, S.: Global evaluation of ammonia bidirectional exchange and livestock diurnal variation schemes, *Atmos. Chem. Phys.*, 15, 12 823–12 843, doi:10.5194/acp-15-12823-2015, 2015.
- 1055

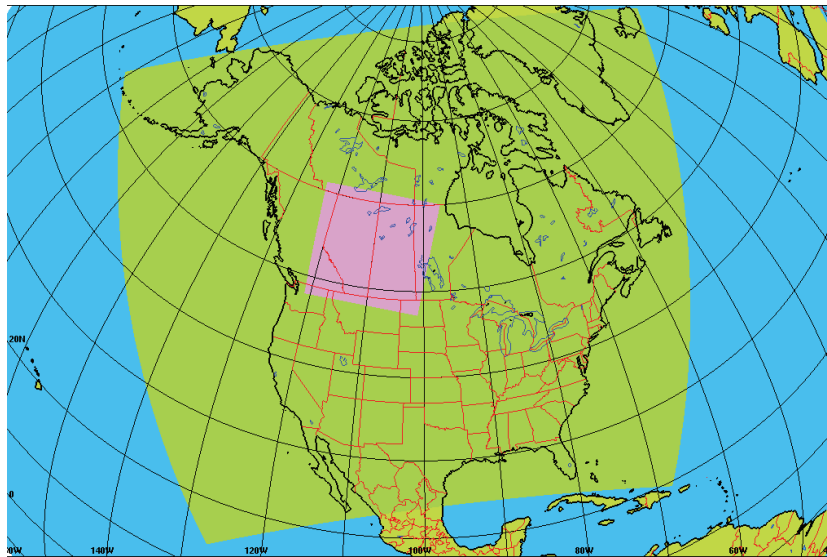


**Figure 2.** Map of 10-km resolution continental piloting model domain (green), and 2.5-km resolution nested model domain (purple).

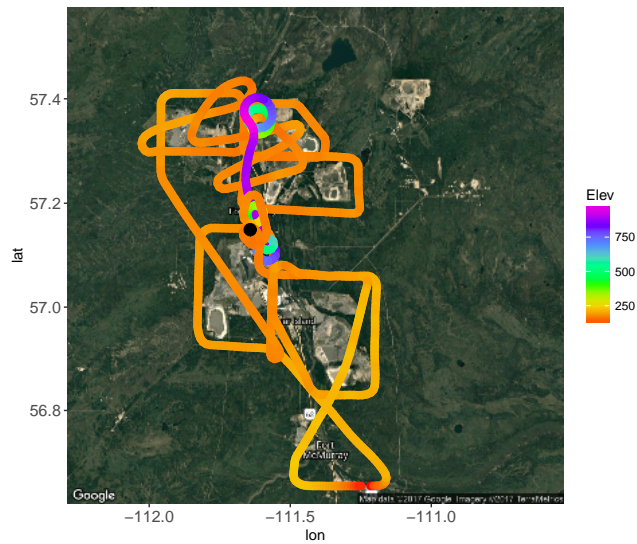


**Figure 3.** Flight path on 13 August 2013, where elevation (in meters) is denoted by the colour scale, and the AMS13 site is indicated by a black circle.

Surface concentrations at Oil Sands AMS13 site

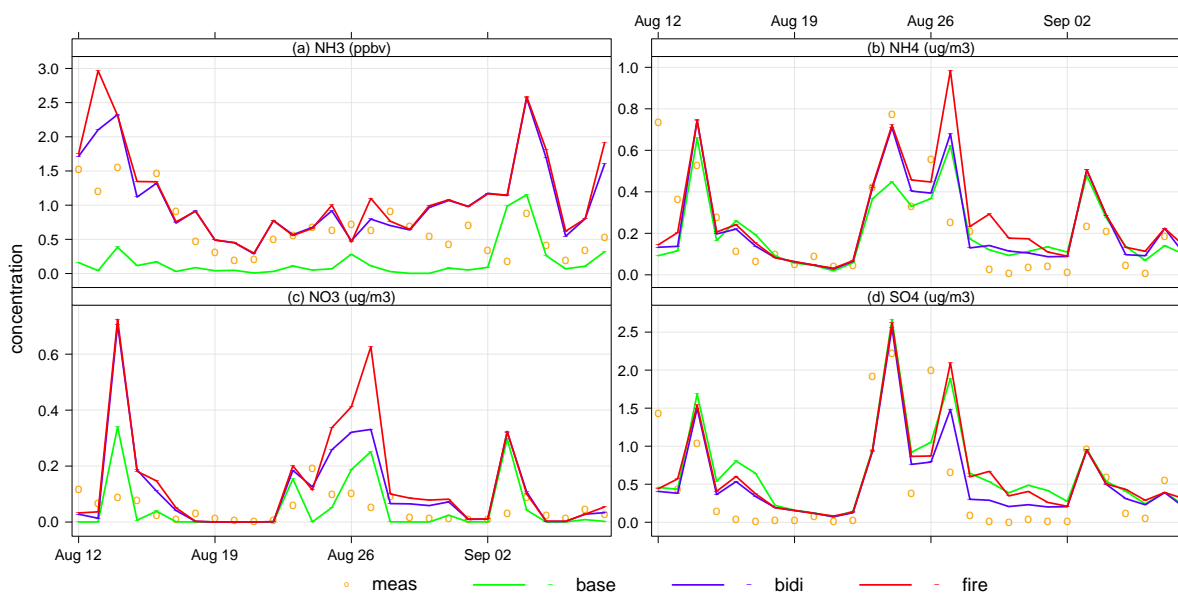


**Figure 4.** Surface daily average (a)  $\text{NH}_3$ , (b) fine particulate  $\text{NH}_4^+$ , (c)  $\text{NO}_3^-$ , and (d)  $\text{SO}_4^{2-}$  concentrations at the AMS13 ground site in the AOSR. Measurements in orange, base model in green, bidirectional flux model in blue, and fire+bidirectional flux model in red.

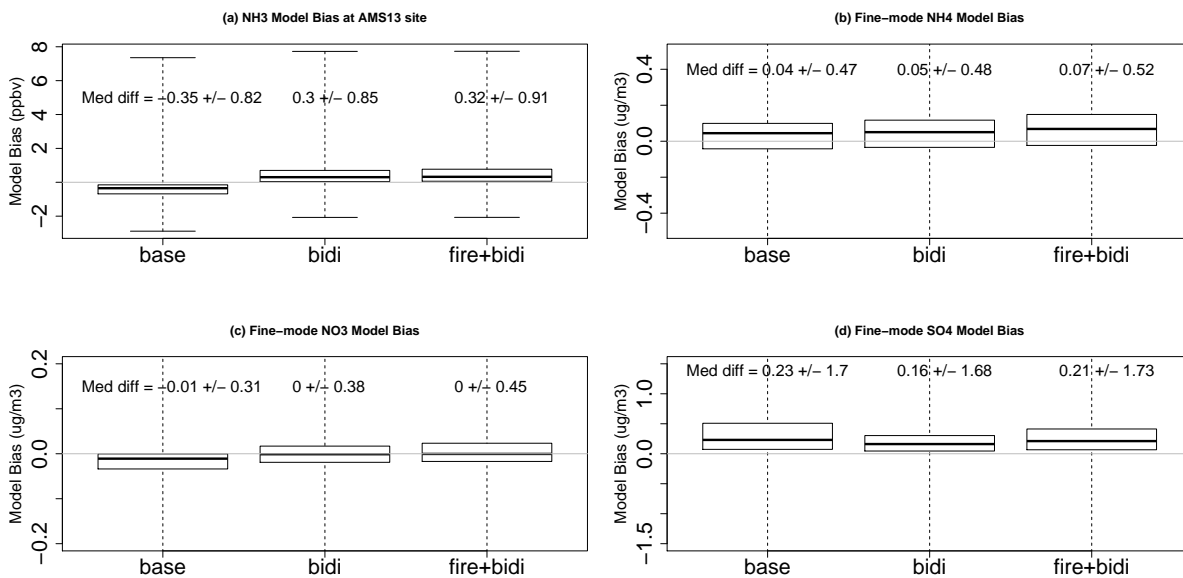


**Figure 5.** Hourly model-measurement bias in surface (a)  $\text{NH}_3$ , (b)  $\text{NH}_4^+$ , (c)  $\text{NO}_3^-$  and (d)  $\text{SO}_4^{2-}$  concentrations at the AMS13 ground site in the AOSR.

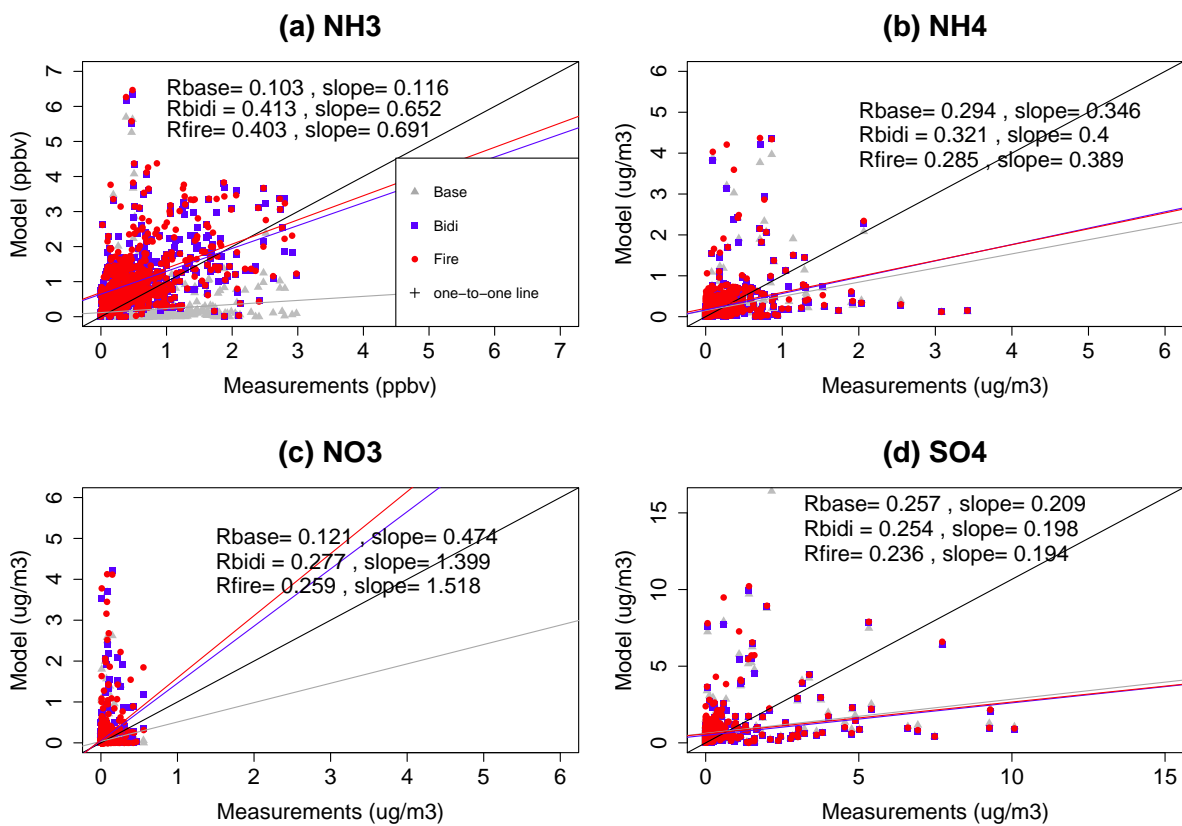
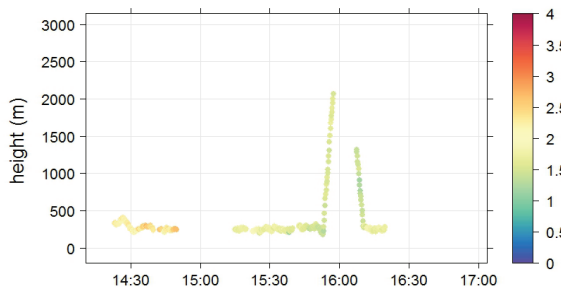
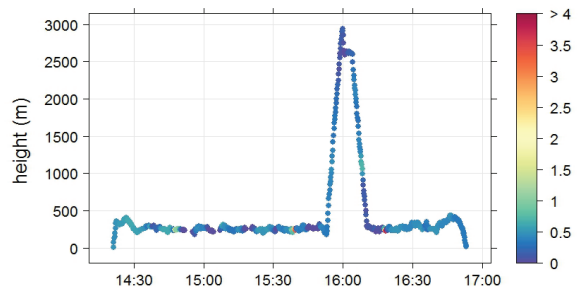


**Figure 6.** Hourly modelled vs measured surface (a) NH<sub>3</sub>, (b) NH<sub>4</sub><sup>+</sup>, (c) NO<sub>3</sub><sup>-</sup> and (d) SO<sub>4</sub><sup>2-</sup> concentrations at the AMS13 ground site in the AOSR. Base model in grey, bidirectional flux model in blue, and fire+bidirectional model in red.

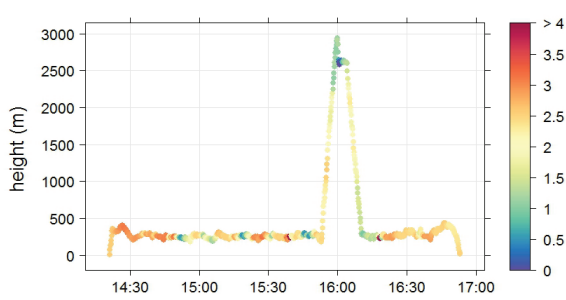
(a) Aircraft NH<sub>3</sub> Measurements at the Oil Sands



(b) Aircraft NH<sub>3</sub> Base Model at the Oil Sands



(c) Aircraft NH<sub>3</sub> Bidi+Fire Model at the Oil Sands



(d) Aircraft NH<sub>3</sub> Bidi Model at the Oil Sands

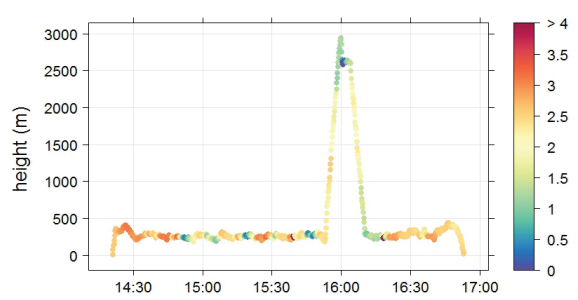


**Figure 7.** NH<sub>3</sub> concentrations aloft (colour scale) over the OS region during the 13 August 2013 flight. (a) measurements, (b) base model, (c) fire+bidi model, and (d) bidi model.

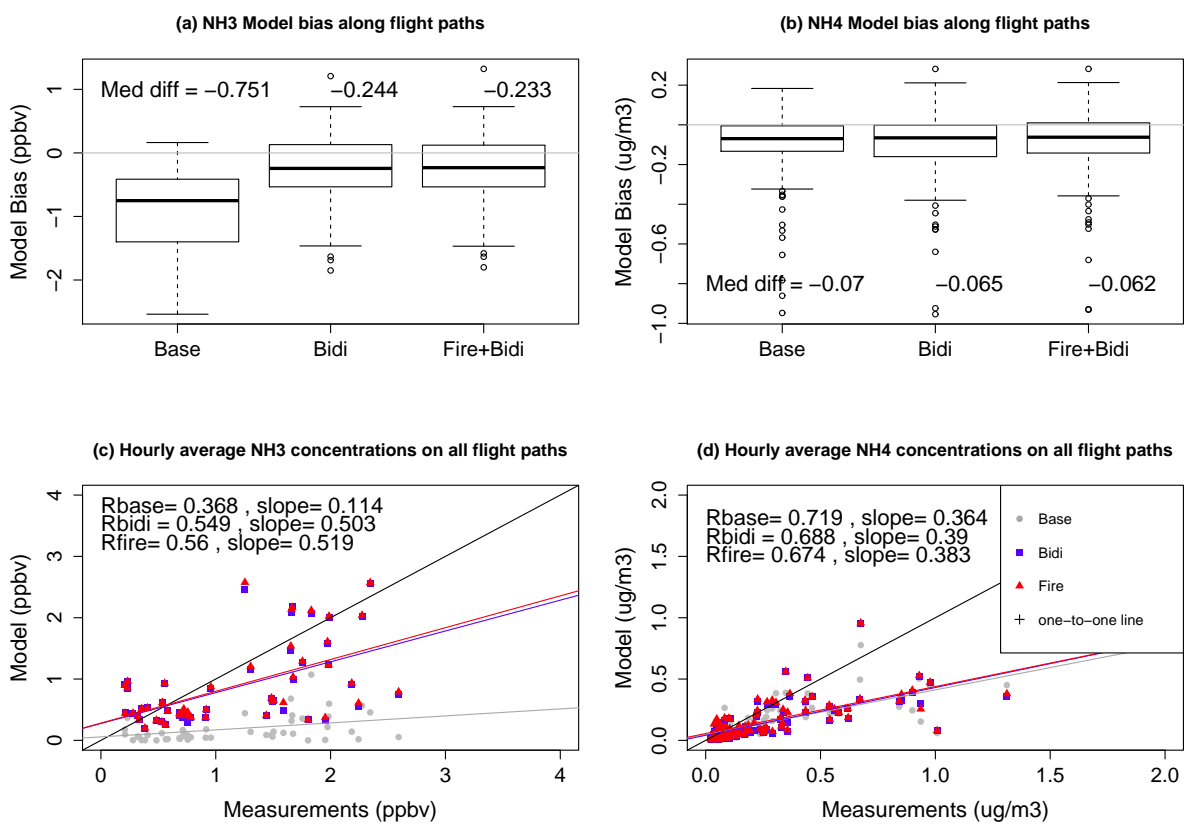


**Figure 8.** Hourly averages along all flight paths over the OS region during the summer 2013 campaign: Model-measurement bias in (a)  $\text{NH}_3$  and (b)  $\text{NH}_4^+$ . Modelled vs measured (c)  $\text{NH}_3$  and (d)  $\text{NH}_4^+$  concentrations aloft. Base model in grey, bidirectional flux model in blue, and fire+ bidi model in red.

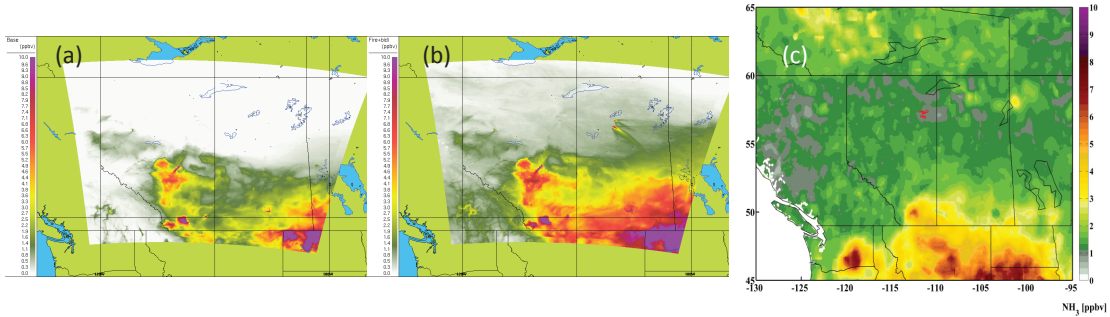
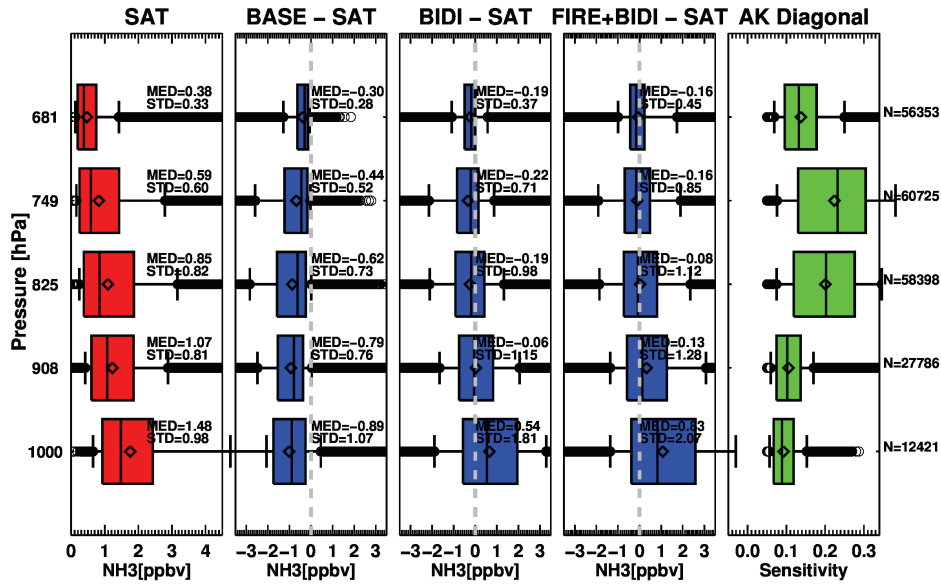


**Figure 9.** Top panel: (a)  $\text{NH}_3$  vertical profile as measured by CrIS satellite, difference between measurement and (b) base model, (c) bidi model, and (d) fire+bidi model, and (e) averaging kernel of CrIS satellite for  $\text{NH}_3$  retrieval. Bottom panel: average (12 Aug - 7 Sep 2013) surface  $\text{NH}_3$  concentrations given by the (a) base model, (b) fire+bidi model, and (c) CrIS satellite.

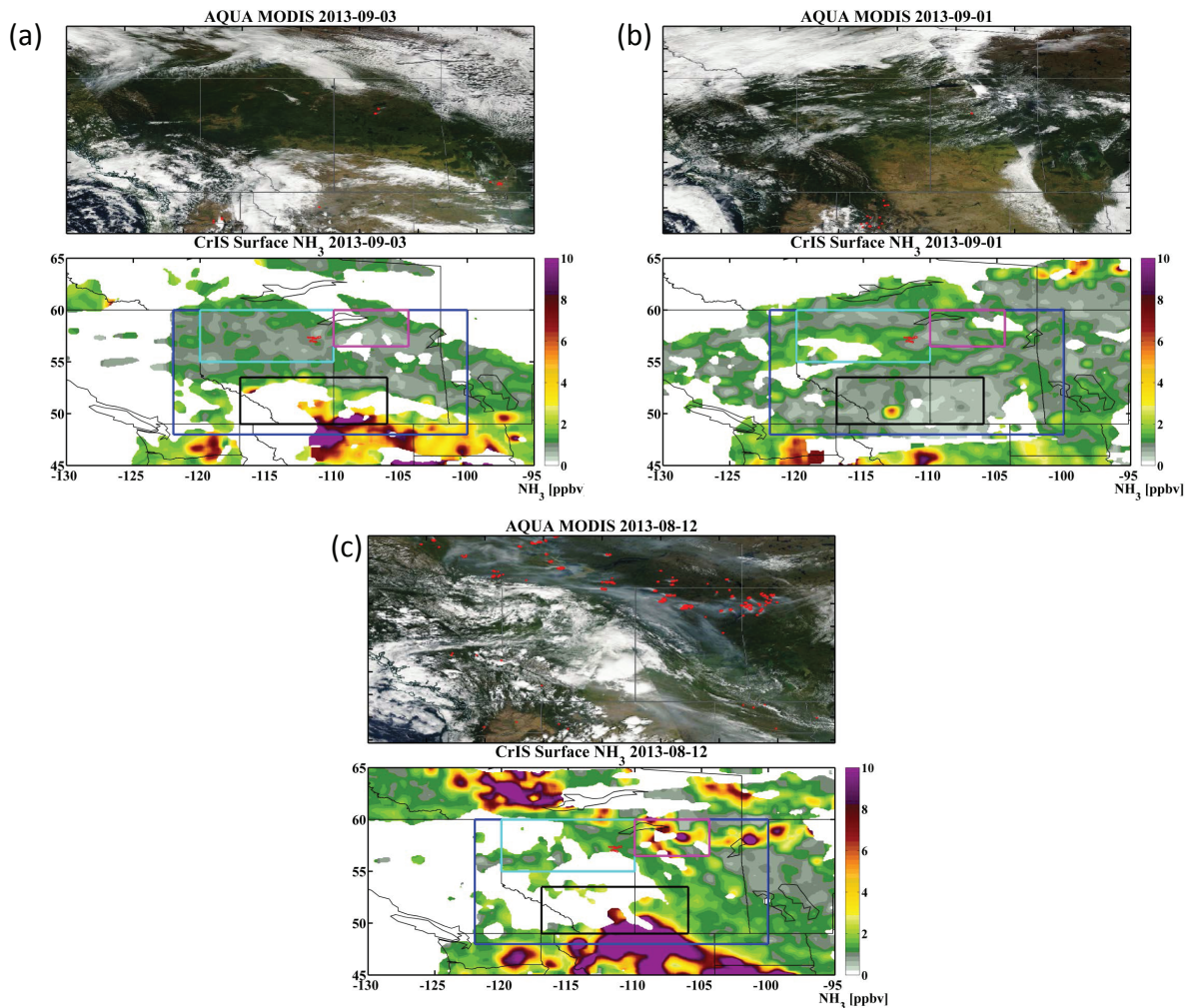


**Figure 10.** (Top panels) Images of the Alberta/Saskatchewan region with clouds and fire hotspots from MODIS. (Bottom panels) Map of CrIS-measured surface  $\text{NH}_3$  concentrations, with coloured boxes showing the regions where model and satellite measurements were sampled. These three examples are for (a) northern bidi case study (cyan), (b) southern bidi case study (black), and (c) fire case study (magenta), discussed in Section 4.3, and the blue box is the region of our overall comparison.

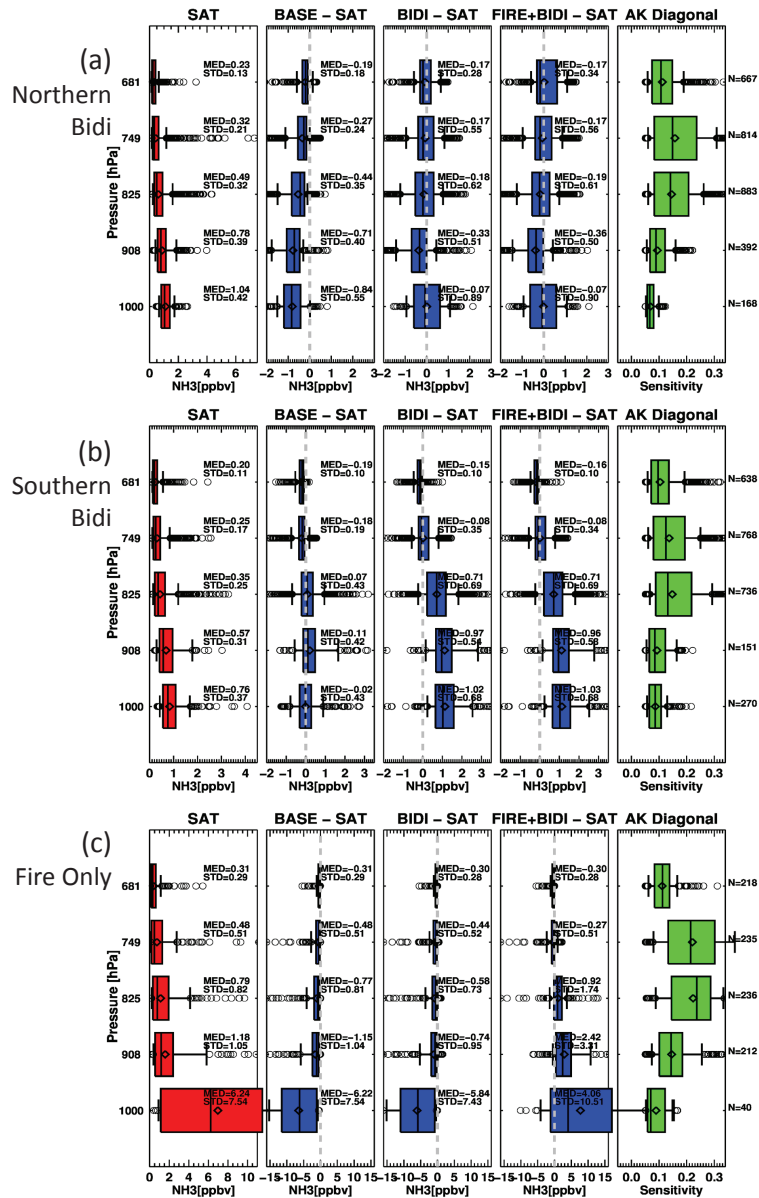


**Figure 11.** As in Fig. 9, but for our (a) northern “bidi-only” case study (3 Sept 2013), (b) southern “bidi-only” case study (1 Sept 2013), and (c) northern “fire-only” case study (12 Aug 2013). Regions are shown in Figure 10a (cyan), 10b (black), and 10c (magenta) boxes, respectively).

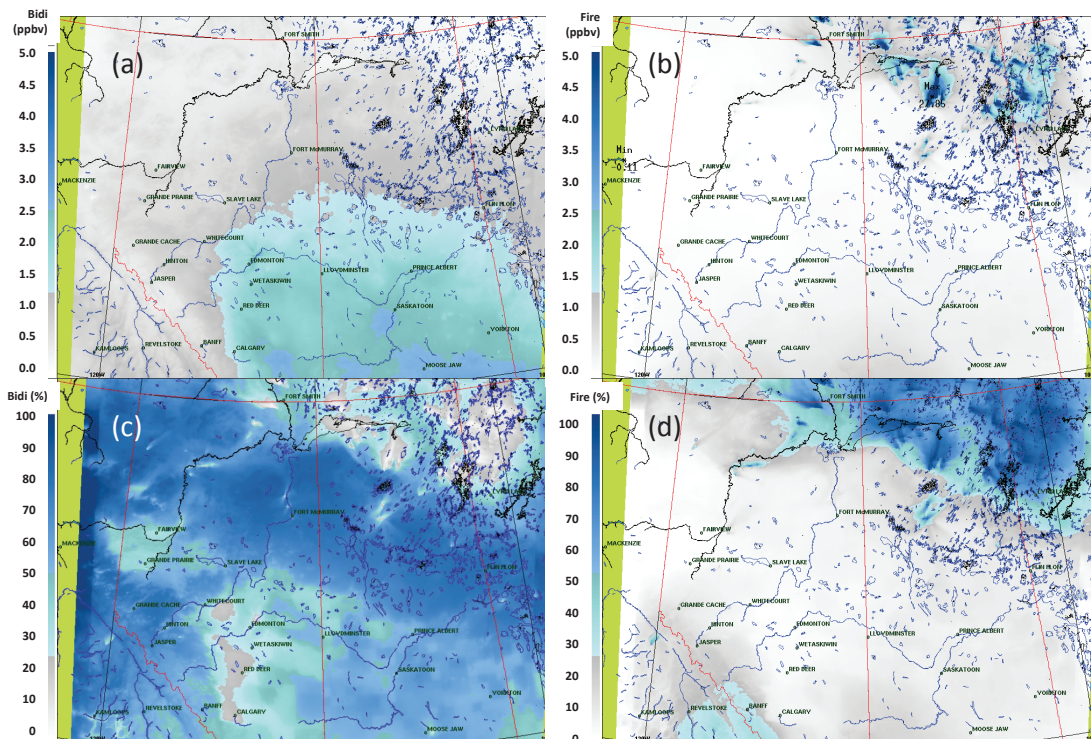


**Figure 12.** Maps of the modelled (a) absolute bidirectional flux contribution, (b) absolute fire contribution, (c) percent bidirectional flux contribution, and (d) percent fire contribution to surface  $\text{NH}_3$ . These are averages over 12 August to 7 September, 2013.

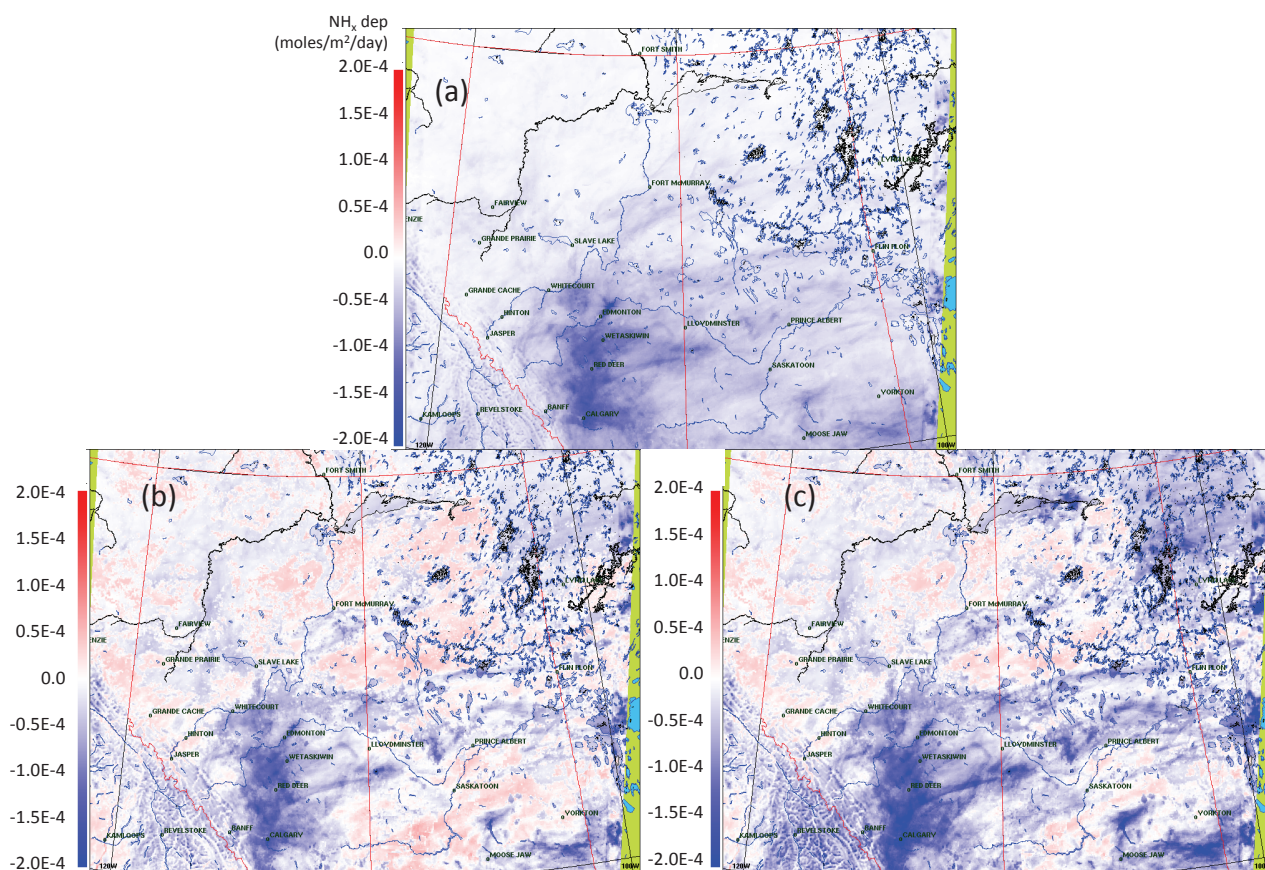


**Figure 13.** Maps of the modelled average  $\text{NH}_x$  deposition for (a) base (b) bidi, and (c) fire+bidi models. In all maps, red/positive represents upward flux, and blue/negative represents downward flux. These are daily amounts, averaged over 12 August to 7 September, 2013.

**Table 2.** Model-measurement NH<sub>3</sub> comparison statistics from 12 August to 7 September 2013: R=correlation coefficient; slope is of the line-of-best fit between model vs. measurement; p and t are from a paired t-test between model and measurement data pairs (p>0.05 and |t|<1 means that the model is statistically indistinguishable from measurements); the median model bias; RMSE=root-mean-square error; and FE=fractional error of the models. CrIS (troposphere) results are for the entire model domain at all tropospheric levels shown in Figure 9(top), and CrIS (surface) results are for the lowest retrieval level (both are during mid-day satellite overpass times); aircraft results are from the 12 flight paths over the oil sands facilities, hourly averages during the daytime; and AMS13 results are from hourly data (day and night) at the one ground station.

	R	slope	p	t	bias (ppbv)	RMSE (ppbv)	FE
<b>CrIS (troposphere)</b>							
base	0.248	0.076	<2E-16	-247.5	-0.430	2.02	-5.3E-6
bidi	0.302	0.205	<2E-16	-77.4	-0.176	1.93	-1.2E-6
fire+bidi	0.338	0.425	<2E-16	36.2	-0.126	2.45	5.9E-7
<b>CrIS (surface)</b>							
base	0.272	0.118	<2E-16	-19.0	-1.11	5.72	-1.6E-3
bidi	0.289	0.162	<2E-16	-12.8	-0.66	5.32	-8.9E-4
fire+bidi	0.566	1.195	1.4E-06	4.9	-0.19	8.67	3.7E-4
<b>aircraft (hourly)</b>							
base	0.368	0.114	8.5E-14	-10.3	-0.751	1.14	-2.5E-3
bidi	0.549	0.503	0.0026	-3.2	-0.244	0.69	-5.0E-4
fire+bidi	0.560	0.519	0.0052	-2.9	-0.233	0.68	-4.5E-4
<b>AMS13 (hourly)</b>							
base	0.103	0.116	<2E-16	-12.4	-0.35	0.92	-1.6E-3
bidi	0.413	0.652	<2E-16	12.1	-0.30	0.95	8.0E-4
fire+bidi	0.403	0.691	<2E-16	13.1	0.32	1.04	9.0E-4

**Table 3.** Average source contributions to ambient NH<sub>3</sub> concentrations over the AB/SK model domain during 12 Aug to 7 Sep 2013.

source	median (ppbv)	median (%)	average (ppbv)	average (%)
total surface NH <sub>3</sub>	1.60	100	2.53	100
from fires to surface	0.25	10.4	0.42	20.3
from bidi to surface	0.97	56.3	1.24	56.6
from anthro to surface	0.38	33.3	0.87	23.1
total column NH <sub>3</sub>	18.8	100	25.6	100
from fires to total column	6.1	27.7	8.1	30.5
from bidi to total column	8.8	48.1	11.15	50.0
from anthro to total column	3.9	24.2	6.35	19.5

**Table 4.** Average  $\text{NH}_x$  deposition (downward flux) over the AB/SK model domain during 12 Aug to 7 Sep 2013.

Net Flux (moles/m <sup>2</sup> /day)	base	bidi	fire+bidi
mean	$3.025 \times 10^{-5}$	$1.811 \times 10^{-5}$	$3.765 \times 10^{-5}$
median	$2.061 \times 10^{-5}$	$1.299 \times 10^{-5}$	$2.843 \times 10^{-5}$